Master's thesis

2021

Kevin Kottakkakathu Varughese

NTNU
Norwegian University of
Science and Technology
Faculty of Natural Sciences
Department of Chemistry

NTNU
Norwegian University of
Science and Technology

Kevin Kottakkakathu Varughese

Nanothermodynamics of a Single-Phase Fluid Confined in a Complex Porous Medium

June 2021

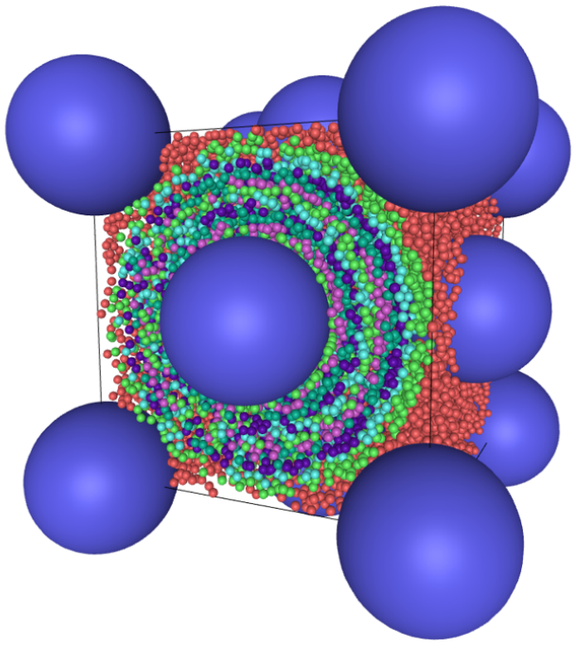

NTNU
Norwegian University of
Science and Technology

NTNU

Norwegian University of
Science and Technology

Nanothermodynamics of a Single-Phase Fluid Confined in a Complex Porous Medium

Kevin Kottakkakathu Varughese

MTNANO
Submission date: June 2021
Supervisor: Signe Kjelstrup
Co-supervisor: Olav Galteland
Michael Tobias Rauter

Norwegian University of Science and Technology
Department of Chemistry

Nanothermodynamics of a Single-Phase Fluid Confined in a Complex Porous Medium

Kevin Kottakkakathu Varughese

CC-BY 2021/06/21

Preface

The work was carried out with guidance and close cooperation with my supervisor Professor Signe Kjelstrup, and co-supervisors PhD candidate Olav Galteland and Michael Tobias Rauter. The Lennard Jones/Spline plugin for LAMMPS is developed and maintained by Olav galteland. Most of the theory for this work is based on papers published by Olav Galteland, Professor Signe Kjelstrup and other great minds working at PoreLab. The work is an attempt at expanding prior work by Galteland and coworkers.

The author thanks his supervisors for the guidance, understanding and patience. It has been of great comfort through the entire study.

Abstract

Nanothermodynamic theories and ideas are applied to a porous medium using Monte Carlo simulations with molecular dynamics based on grand canonical ensemble. Initially the theory is tested against a slit pore, thereafter expanded upon to be used with a porous membrane where the solid particles are defined by a Face-Centered Cubic Lattice. Ensembles of FCC unit cells are constructed, following Grand Canonical ensemble properties, i.e controlled temperature, volume, surface area and chemical potential. For the slit pore, Integral and differential properties at small system scale as introduced by Hill, is looked into. Simulations are carried out with either varying chemical potential or varying height, keeping other properties constant in the case of slit pore. This lets us study the effects of chemical potential and volume on slit pores according to nanothermodynamic description of the slit pore. Regardless of the pathway chosen to describe specific properties, the results seem to be similar, suggesting the nanothermodynamic description is consistent. After testing the theory against the slit pore, we expand upon it to find an alternate route to describe the integral pressure of single-phase fluid in porous membrane. We test the new method controlling for temperature, volume and chemical potential, and study how well the integral pressure is described. After evaluating the yielded results, the alternate route described in this paper seem to give satisfactory results when compared against values from other work.

Sammendrag

Nanotermodynamiske teorier og ideer blir her brukt på små systemer, spesifikt et porøsmedium, ved hjelp av Monte Carlo simulasjoner med Molekylær Dynamikk basert på "Grand Canonical Ensemble". Til å begynne med tester vi teorien mot spaltepore, deretter ekspanderer vi teorien og ligninene til å passe til bruk med porøsmembran. Det porøse mediumet som blir brukt her består solide partikler satt sammen som en "Face-Centered Cubic lattice". Flere tilfeller av FCC enhetscellene blir her konstruert i forhold til "Grand Canonical Ensemble" egenskaper, altså at temperatur, volum, overflate, areal og kjemiskpotensial blir kontrollert. For tilfellet hvor vi studerer spalteporet, ser vi på integral og differensial egenskaper av småsystemer, som beskrevet av Hill. For spalteporet er simulasjoner med varierende høyder og kjemiskpotensial kjørt, og resten av egenskapene ble holdt konstant. Dette lot oss studere hvordan kjemiskpotensiale og høyde påvirker småsystemer i forhold til nanotermodynamiske beskrivelser, ihvertfall for spalteporer. Vi så at vi kom til lignende resultater uavhengig av hvilken metode vi valgte å studere egenskapene. Dette viser til at det nanotermodynamiske beskrivelsen er konsistent. Deretter videreførte vi teorien til å passe med porøs medium. Vi ville beskrive integraltrykket til enfaset væske i porøs medium, ved å bruke en ny metode. Så testet vi den nye metoden ved å kontrollere for temperatur, volum og kjemiskpotensial. Deretter studerte vi hvor godt integraltrykket kan beskrives av metoden. Til slutt evaluerte vi resultatene, og det viser seg at den alternative eller nye metoden som blir beskrevet her gir tilfredstilende resultater når det sjekkes opp mot verdier fra andres arbeid.

Contents

Figures

Tables

Chapter 1

Introduction

The change in thermodynamic properties as one moves towards a small system is well known [1], but not used by many. Leaving an underused opportunity for further work. Efforts have been made to thermodynamics to work with systems of this scale as well [2]. There are several small systems one could consider. A slit pore, for instance a fluid phase confined between two solid phases, is a system we worked on for preliminary work. Further work was then conducted on a system made up of fluid in porous medium, the porous medium being a single FCC unit cell. Applying the work so far related to nanothermodynamics on such a system could yield valuable insights such as how well the nanothermodynamic description works, or understanding studying flow at nano-scale to be able to use acquired knowledge on up-scaling to Darcy´s scale.

Slit pores are in themselves important models that could represent important real life applications. Examples of such could be thin-films for instance in fuel cells and batteries. Better understanding of such systems could be beneficial in our quest to advancing related technologies. Nanothermodynamics can help with providing such systems the thermodynamic description that could help research in those fields. After showing that the nanothermodynamic description of slit pore is viable the way we set it up, further work is then focused towards the FCC porous medium.

The thermodynamic description of transport processes in porous medium poses several challenges as described in literature [3–8]. Using the nanothermodynamic framework as described in literature [2], we try to describe the pressure of immiscible fluids in porous medium. This is especially interesting because there cur-

rently is no consensus regarding the definition, measurement or calculation of such [3]. One can use microscopic pressure tensor, but this is ill-defined and the problem is enhanced in heterogeneous systems with interfaces between solids and fluid [3]. For the FCC unit cell we use here as the porous medium, we have curved surfaces of solid particles as well as fluid confinement. Making it difficult to apply accepted methods for calculation of microscopic pressure tensor, and in turn the pressure gradient that could act on fluid flow.

The main goal here is to use the nanothermodynamic framework as described in literature [2] to possibly find an alternative method, and preferable a less problematic one as described earlier, to describe the pressure in heterogeneous small systems. By doing this, provide further data and insight into previous work. The work here is related to paper published by Galteland et al. [3], however trying to solve the issue using a new method. We describe the integral pressure as a function of chemical potential. The work seem to indicate that the method yields results that are consistent with observations from prior work and was tested against reference values provided by a fellow Master student who was also doing related work.

Chapter 2

Theory

One of the main features of thermodynamics is its ability to describe the conversion of energy. Two processes that can be described as transfer of energy is work and heat. And they're both connected to each other. When work is done by a thermodynamic system, it loses heat. Under the first law, when work is done on the system, it gains heat. A real life example of this that many could relate to is using a bicycle pump, trying to pump, one would be able to experience heat generating.

Together, the work and heat transferred into or out of the system represents the change in its total energy, also commonly referred to as internal energy. This idea is so fundamental, that the first law of thermodynamics is that the internal energy is equal to the change in work plus the change in heat. As illustrated in the following equation:

$$\Delta U = Q - W. \tag{2.1}$$

ΔU in equation (2.1) denotes the change in the internal energy of a system, Q denotes the quantity of energy supplied to the system as heat, and W denotes the amount of work done by the system on surroundings.

The equation 2.1 can be formulated to describe internal energy based on temperature, pressure, entropy and volume [9]:

$$dU = TdS - pdV. \tag{2.2}$$

Equation (2.2) shows an equivalent equation to equation (2.1) however here measurable change in internal energy, U, is given in terms of entropy, S, and volume, V.

In a closed system one could think transfer of work, due to change in volume, and heat to be the only relevant factors affecting the internal energy of a system. This is however not how it is realistically. A system would be subject to several more factors from its environment, and the variables in the system itself tend also to be more complex.

Gibbs extended the equation discussed so far with the term μ_j, which stands for chemical potential of component j in a mixture of n components. Thus the introduction of μ_j is as a measure of the change in the internal energy due to the change in the amount N_j of component j, as all other quantities are kept constant. Gibbs´ equation is thus given in equation (2.3):

$$dU = TdS - pdV + \sum_{j=1}^{n} \mu_j dN_j. \tag{2.3}$$

The chemical energy is essentially energy that can be absorbed or released due to change of the number of particles of interest.

Thermodynamics so far seem fine from a macroscopic level. However, when one moves from a macroscopic number down to a few molecules, the normal thermodynamic relations cease to apply [2]. A systematic theory was already proposed in 1960s to deal with issues arising from the problem previously mentioned, that normal thermodynamic relations cease to apply at systems too small [1].

Here we delve deeper into this proposed systematic theory, calling it nano-thermodynamics, by applying it to a single-phase fluid in a slit pore, and then to a porous medium with FCC structure. We do this by using grand canonical Monte Carlo and molecular dynamics. The slit pore system itself will consist of solid walls, with varying variables consistent with grand canonical ensemble (see section 2.2). The porous medium will consist of solid walls defining a single FCC unit cell.

See figure (2.1) for an illustration of a slit pore. The blue area in this figure is essentially the area of the simulation box, example of such a simulation box can be seen in figure (4.1).

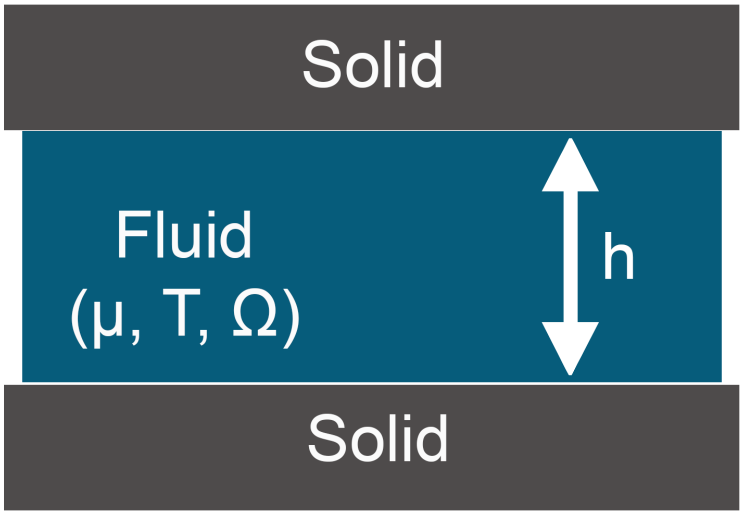

Figure 2.1: Diagram of a slit pore. The diagram highlight some of the ensemble values that are considered in this work; Chemical potential μ, Temperature T, surface area Ω, height h.

2.1 Nanothermodynamics

As suggested in the introduction, energy conversion cannot be described without the laws of thermodynamics. However, while classical thermodynamics is useful for describing systems with a large number of particles [2], it is less so for a system of small number of particles. One can perhaps differentiate [2] a large system from a small one by defining as follows: A system can be considered large, in the thermodynamic sense, when the thermodynamic variables U, S, and N are proportional to the volume of the system. Thus, it follows that the total energy of two large systems combined into one system is then equal to the sum of the energy of the initial two systems separate. The system is extensive. Meanwhile, a system is to be considered small, in the thermodynmaic sense, when the total energy of two small systems combined is not equal to the sum of the energy of

the two separate small systems.

The variables in equations (2.2) and (2.3) are extensive, in other words; proportional to the volume of the system. The internal energy U is an Euler homogeneous function of degree one of S, V, and N_j. Leading to the equation(2.3) being a total differential in the variables.

Small systems, we see, have non-extensive variables. There will be a substantial contribution to U, S, and N, proportional to the surface area ($\sim V^{2/3}$), as a system becomes smaller [2]. There are also contributions proportional to $V^{1/3}$ and constant contributions, if the surface tension depends on the surface curvature, or if the surface has edges and nooks.

Hill proposed a procedure that enabled one to take advantage of the systematic structure of thermodynamics while also being able to describe the energy conversion under small system conditions [1]. Hill did this by introducing an ensemble of replicas of small systems, rather than looking at *one* small system. By doing this, one could use normal thermodynamic relations for the ensemble, and then compute the average properties of the small systems in the ensemble. Thus, leading to the following equation, also referred to as Hill-Gibbs equation [2]:

$$dU_t = TdS_t - pdV_t + \sum_{j=1}^{n} \mu_j dN_{j,t} + \epsilon d\mathcal{N}. \tag{2.4}$$

The subscript t in equation (2.4) indicates that it is an ensemble property, i.e the total value of the whole ensemble of replicas. Number of replicas $\mathcal{N}$ was introduced to equation (2.3). ϵ, denotes the replica energy or subdivision potential, which is the energy associated with the increase in the total internal energy when one replica is added to an ensemble. All while keeping the total entropy S_t, total volume V_t and the total amounts $N_{j,t}$ constant. This can be different for a different set of controlled variables. The properties of the ensemble becomes Euler homogeneous of degree one in the number of replica, and it remains extensive, when these conditions are met. So, by construction, the ensemble variables U_t, S_t, N_t, $\mathcal{N}$ are Euler homogeneous functions of first order. From equation (2.4) one can formulate the following equation for the total differential of U_t:

$$dU_t = TdS_t - pdV_t + \mu \cdot d\mathrm{N}_t + \epsilon d\mathcal{N}. \tag{2.5}$$

We can further define the temperature T, pressure p, chemical potential μ and

subdivision potential ϵ from the partial derivatives of U_t:

$$\begin{aligned} \left(\frac{\partial U_t}{\partial S_t}\right)_{V_t,\mathrm{N}_t,\mathcal{N}} &= T, \quad \left(\frac{\partial U_t}{\partial V_t}\right)_{S_t,\mathrm{N}_t,\mathcal{N}} = -p, \\ \left(\frac{\partial U_t}{\partial \mathrm{N}_t}\right)_{S_t,V_t,\mathcal{N}} &= \mu, \quad \left(\frac{\partial U_t}{\partial \mathcal{N}}\right)_{S_t,V_t\mathrm{N}_t} = \epsilon. \end{aligned} \tag{2.6}$$

By integrating the differential at equation (2.5) for total internal energy U_t by holding constant the temperature T, pressure p, chemical potential μ and subdivision potential ϵ, we get a revised Euler equation:

$$U_t = TS_t - pV_t + \mu \cdot \mathrm{N}_t + \epsilon\mathcal{N}. \tag{2.7}$$

Differentiating equation (2.7) and using equation (2.5) and averaging it over the number of replicas by dividing it by $\mathcal{N}$, we get the equation we refer to as Hill-Gibbs-Duhem equation:

$$d\epsilon = -SdT + Vdp - \mathrm{N} \cdot d\mu. \tag{2.8}$$

2.2 Representative Elementary Volume

Representative Elementary Volume (REV) is a central element in the derivation of the equations of transport on the macro-scale is the definition of a representative elementary volume (REV) [3]. The size of the REV should be large compared to the pore size and small compared to size of the porous medium, and contain a statistically representative collection of pores. In essence REV is the smallest volume over which a measurement can be made that will yield a representative value for the whole [1]. REV is essential in a macro-scale description. Rev makes it possible to obtain thermodynamic variables on the macro scale. Galteland et al. [3] discusses how constant macro-scale pressure in equilibrium makes it possible to obtain the integral pressure in the solid, and the surface tension of the liquid-solid contacts in REV.

2.3 Grand Canonical Ensemble

The environment variables we will consider to keep constant or vary in order to study the differences in their contribution to system effects will be T, V and μ. The

possible exchanges with the environment when considering such a system would be its internal energy U and particles N_j. The environmental variables V, T, μ and the shape are used as variables to define the grand canonical ensemble (GC).

Since V_t is an ensemble property that means the total volume of all the $\mathcal{N}$ replicas in the ensemble, it follows that $V_t = \mathcal{N}V$. Inserting this into equation (2.5) we get for GC:

$$\begin{aligned} dU_t &= TdS_t - p\mathcal{N}dV + \mu \cdot d\mathrm{N}_t + (\epsilon - pV)d\mathcal{N} \\ &= TdS_t - p\mathcal{N}dV + \mu \cdot d\mathrm{N}_t + Xd\mathcal{N}. \end{aligned} \tag{2.9}$$

Note from equation (2.9) that the replica energy X for GC is:

$$X(T,V,\mu) = \epsilon - pV. \tag{2.10}$$

Which is also equal to the specific internal energy of the ensemble of replicas:

$$X(T,V,\mu) = \left(\frac{\partial U_t}{\partial \mathcal{N}}\right)_{S_t, V\mathrm{N}_t}. \tag{2.11}$$

In other words, at constant S_t, V, N_t, and shape, the replica energy stands for the reversible work needed to add one replica of the small system to the ensemble. This also means that, considering how the ensemble properties are kept constant when adding a replica, these values need to be redistributed over the replicas. Meanwhile the total volume V_t increases.

For the GC ensemble replica energy X as $-\widehat{p}V$, as denoted by Hill [1]. This is because replica energy for GC is a quantity that can be associated with work. In classical thermodynamics, work can normally done by extending volume. Work here can also be done when the number of replicas increases. As this operation is additive, Hill introduced the term "Integral pressure", or p-hat, for $\widehat{p}$ [1]. It thus becomes custom to call $\widehat{p}$ as the integral pressure, and p the differential pressure henceforth. We thus define the following from equation (2.11):

$$\widehat{p}(T,V,\mu) \equiv -X(T,V,\mu) = -\left(\frac{\partial U_t}{\partial \mathcal{N}}\right)_{S_t, V\mathrm{N}_t}. \tag{2.12}$$

Integrating the differential given in equation (2.9) by holding temperature T, volume V and chemical potential $\boldsymbol{\mu}$, we get the following:

$$\begin{aligned} U_t(T,V,\mu,\mathcal{N}) &= TS_t(T,V,\mu,\mathcal{N}) \\ &\quad + \mu \cdot \mathrm{N}_t(T,V,\mu,\mathcal{N}) - \widehat{p}(T,V,\mu)V\mathcal{N}. \end{aligned} \tag{2.13}$$

For the small systems or replicas, the average values for internal energy U, entropy S and particles N_j of type j, are related to the ensemble values as follows:

$$\begin{aligned} U_t(T,V,\mu,\mathcal{N}) &\equiv \mathcal{N}U(T,V,\mu), \\ S_t(T,V,\mu,\mathcal{N}) &= \mathcal{N}S(T,V,\mu), \\ N_{j,t}(T,V,\mu,\mathcal{N}) &\equiv \mathcal{N}N_j(T,V,\mu). \end{aligned} \tag{2.14}$$

The entropy S is determined by the probability distribution over N and U, these would be the same for each replica in the ensemble.

By combining variables in equation (2.14) to equation (2.10) and introducing them to equation (2.13), we get the following:

$$\begin{aligned} X(T,V,\mu) &= -\widehat{p}(T,V,\mu)V \\ &= U(T,V,\mu) - TS(T,V,\mu) - \mu \cdot \mathrm{N}(T,V,\mu). \end{aligned} \tag{2.15}$$

From equation (2.15) one can observe that internal energy U for GC is not an Euler homogeneous function of degree one in entropy S, volume V and particles N. A replica or small system will only follow classical thermodynamics if differential pressure and integral pressure is the same, $\widehat{p} = p$. The difference between differential pressure p and integral pressure $\widehat{p}$ multiplied by the volume V gives us the subdivision potential ϵ:

$$(p - \widehat{p})V = \epsilon. \tag{2.16}$$

By the definition, mentioned earlier for small vs large system, it follows that a system is small when $\widehat{p} \neq p$. A factor that contributes to this difference between integral pressure $\widehat{p}$ and differential pressure p is surface energy [10]. Inserting variables from equation (2.14) into equation (2.9), combining equation (2.15), we get the Gibbs relation for a replica, or the small system:

$$dU = TdS - pdV + \mu \cdot d\mathrm{N}. \tag{2.17}$$

Which leads us to the corresponding Hill-Gibbs-Duhem equation for GC:

$$d(\widehat{p}V) = SdT + pdV + \mathrm{N} \cdot d\mu. \tag{2.18}$$

2.3.1 Nanothermodynamics and small systems

We will now begin by applying the nanothermodynamics we have discussed so far to slit pores. We do this by considering an ensemble of $\mathcal{N}$ slit pore replicas, where each pore is filled with a single-phase and -component fluid. The replicas do not react with each other. Slit pore j in the ensemble consists of two parallel plane walls with area Ω_j with distance h_j between the parallel walls. The walls being plane, have no volume. The total volume V_t of the ensemble is then given by:

$$V_t = \sum_{j=1}^{\mathcal{N}} h_j \Omega_j. \tag{2.19}$$

Also note that the total surface area is:

$$2\Omega_t = 2\sum_{j=1}^{\mathcal{N}} \Omega_j. \tag{2.20}$$

Note that the "2" in equation (2.20) arises from the fact that in a slit pore the total surface consists of two fluid-solid surfaces of equal area.

The total differential of the internal energy U_t for such an ensemble consisting of slit pore replicas is:

$$dU_t = TdS_t - p_\perp dV_t + 2\gamma d\Omega_t + \mu d\mathrm{N}_t + \epsilon d\mathcal{N}. \tag{2.21}$$

We observe that equation (2.21) is similar to the Hill-Gibbs equation (2.4).

The partial derivatives of equation (2.21), in other words, the partial derivatives of the internal energy gives us the temperature T, normal pressure $p_\perp$, surface tension γ and chemical potential μ:

$$\begin{aligned} \left(\frac{\partial U_t}{\partial S_t}\right)_{V_t,\Omega_t,\mathrm{N}_t,\mathcal{N}} &= T, \quad \left(\frac{\partial U_t}{\partial V_t}\right)_{S_t,\Omega_t,\mathrm{N}_t,\mathcal{N}} = -p_\perp, \\ \left(\frac{\partial U_t}{\partial \Omega_t}\right)_{S_t,V_t,\mathrm{N}_t,\mathcal{N}} &= 2\gamma, \quad \left(\frac{\partial U_t}{\partial \mathrm{N}_t}\right)_{S_t,V_t,\Omega_t,\mathcal{N}} = \mu. \end{aligned} \tag{2.22}$$

We see that this is similar to the partial derivatives mentioned in equation (2.6).

From the partial derivatives in equation 2.22, it follows that the volume is changed by the change in distance between the surfaces: $h_j \equiv V_j/\Omega_j$, when the volume derivative is taken while keeping the total surface area constant. Also note that the change in pore height and surface area is changed in such a way that the

total volume is zero, when the surface derivative is taken keeping the volume constant.

Maxwell relations

We saw that the internal energy of the ensemble or rather the total internal energy is Euler homogeneous of the first order in the number of replicas, in our case slit pores.

If we were to consider the average volume per slit pore $V = V_t/\mathcal{N}$ instead of total volume V_t, and average surface area per slit pore $2\Omega = 2\Omega_t/\mathcal{N}$ instead of total surface area $2\Omega_t$, we could formulate an appropriate Hill-Gibbs equation for this as follows:

$$\begin{aligned} d(V\mathcal{N}) &= \mathcal{N}dV + Vd\mathcal{N}, \\ d(\Omega\mathcal{N}) &= \mathcal{N}d\Omega + \Omega d\mathcal{N}. \end{aligned} \tag{2.23}$$

Combining equation (2.23) with equation (2.21) we get the following equation:

$$dU_t = TdS_t - p_\perp \mathcal{N}dV + 2\gamma\mathcal{N}d\Omega + \mu d\mathrm{N}_t + (\epsilon - p_\perp V + 2\gamma\Omega)d\mathcal{N}. \tag{2.24}$$

Where $\epsilon - p_\perp V + 2\gamma\Omega = X(T, V, \Omega, \mu)$

From equation (2.24) we see that the total internal energy is:

$$U_t = TS_t + \mu\mathrm{N}_t + X\mathcal{N}. \tag{2.25}$$

The average internal energy, entropy and number of particles per slit pore can be seen from the following:

$$\begin{aligned} U_t &= U\mathcal{N}, \\ S_t &= S\mathcal{N}, \\ \mathrm{N}_t &= \mathrm{N}\mathcal{N}. \end{aligned} \tag{2.26}$$

To get the internal energy per slit pore, we can introduce the average properties from equation (2.26) to equation (2.25), so that we obtain the following:

$$U = TS + \mu N + (\epsilon - p_\perp V + 2\gamma\Omega) = TS + \mu N + X. \tag{2.27}$$

Combining the average properties from equation(2.26) into equation (2.24) and using equation (2.27), we get the following equation for the total differential of the internal energy:

$$dU = TdS - p_{\perp}dV + 2\gamma d\Omega + \mu dN. \tag{2.28}$$

Differentiating the internal energy from equation (2.27), then using the total differential of the internal energy from equation (2.28), we get the following equation for the total differential of the replica energy:

$$\begin{aligned} dX &= -d(\widehat{p}_{\perp}V - 2\widehat{\gamma}\Omega) \\ &= -d(\widehat{p}V) \\ &= -SdT - p_{\perp}dV + 2\gamma d\Omega - Nd\mu. \end{aligned} \tag{2.29}$$

The partial derivatives of replica energy from equation (2.29) will present us the following relations:

$$\begin{aligned} \left(\tfrac{\partial(\widehat{p}V)}{\partial T}\right)_{V,\Omega,\mu} &= -\left(\tfrac{\partial X}{\partial T}\right)_{V,\Omega,\mu} &= S, \\ \left(\tfrac{\partial(\widehat{p}V)}{\partial V}\right)_{T,\Omega,\mu} &= -\left(\tfrac{\partial X}{\partial V}\right)_{T,\Omega,\mu} &= p_{\perp}, \\ \left(\tfrac{\partial(\widehat{p}V)}{\partial \Omega}\right)_{T,V,\mu} &= -\left(\tfrac{\partial X}{\partial \Omega}\right)_{T,V,\mu} &= -2\gamma, \\ \left(\tfrac{\partial(\widehat{p}V)}{\partial \mu}\right)_{T,V,\Omega} &= -\left(\tfrac{\partial X}{\partial \mu}\right)_{T,V,\Omega} &= N. \end{aligned} \tag{2.30}$$

Pressure calculations

The slit pore design that is being worked with here, has a translational symmetry in the $y-$ and $z-$direction. The $x-$direction is normal to the solid surface. The equilibrium mechanical pressure tensor in the slit pore is as follows [11]:

$$(x;h) = P_{\perp}(h)_{xx} + P_{\parallel}(x;h)(_{yy} + _{zz}). \tag{2.31}$$

In equation (2.31), $_x$, $_y$ and $_z$ denotes the unit vectors in x-, y- and z-directions. Where the normal pressure tensor component is equal to the xx-component. The tangential pressure tensor component is the average of the yy- and zz-components, as presented in the following set of equations:

$$\begin{aligned} P_{\perp}(h) &= P_{xx}, \\ P_{\parallel}(x,h) &= \tfrac{1}{2}(P_{yy} + P_{zz}). \end{aligned} \tag{2.32}$$

Mechanical equilibrium requires that the tangential pressure is only dependent on the x-coordinate, while the normal pressure is independent of all spatial coordinates. Since the normal mechanical pressure and the area are constant everywhere, one can formulate the thermodynamic integral normal pressure as follows:

$$\widehat{p}_{\perp}(h) \equiv \frac{1}{h}\int_0^h P_{\perp}(h)x = P_{\perp}(h). \tag{2.33}$$

Equation(2.33), the integral normal pressure is be expressed in terms of the volume integral of the normal mechanical pressure divided by the volume. The simplification works because the normal mechanical pressure and the area are constant everywhere.

The integral surface tension is defined as the integral of the normal pressure tensor minus the tangential pressure tensor components as follows [11]:

$$\widehat{\gamma} \equiv \frac{1}{2}\int_0^h (P_{\perp}(h) - P_{\parallel}(x;h))dx. \tag{2.34}$$

The factor $1/2$ in equation (2.34) stems from there being two fluid-solid surfaces in the slit pore. Combining equations (2.29)(2.33)(2.34) one can get to the following equation for integral pressure:

$$\widehat{p}(h) = \frac{1}{h}\int_0^h P_{\parallel}(x;h)dx. \tag{2.35}$$

For integral pressure calculations as a function of chemical potential μ one can derive from equation (2.29) the following:

$$\int_{(\widehat{p}V)_0}^{\widehat{p}V} d(\widehat{p}V) = \int_{\mu_0}^{\mu} N d\mu. \tag{2.36}$$

By setting $\widehat{p}_0 V = 0$, we get the following:

$$\widehat{p}(\mu) = \int_{\mu_0}^{\mu} \rho d\mu. \tag{2.37}$$

Equation(2.37) is the new method we will be using to calculate the integral pressure. In the next section we will expand upon it to be expressed in terms of volume of REV V^{REV}.

2.3.2 Pressure calculation for Porous medium

For this work we focus on the case of a porous medium. The porous medium will be a complex face-centered cubic lattice of solid particles. As with the slit pore the

calculations will be in accordance with the grand canonical ensemble. Expanding on the work by Gatleland et al [3]. The thermodynamic control variables temperature T, porous medium geometry such as lattice constant a and particle radius r, and chemical potential can be varied systematically. The Maxwell relations mentioned in section (2.3.1) was tested for the slit pore and provided promising results that will be discussed later on in this paper. This could be applied to the porous medium as well, focusing on studying the pressure inside the porous medium.

With the slit pore case, we introduced the pressure normal to the pore and the height difference between the walls. However for the porous medium, we have no simple geometry. We keep the term pV in the Euler equation. We also do not introduce the surface area as a variable.

We can use equation(2.13) for the porous medium, in this case an FCC lattice unit cell which is set as the REV:

$$U_t = TS_t + N_{f,t}\mu_f + N_{r,t}\mu_r - \widehat{p}V\mathcal{N}. \tag{2.38}$$

We write the Hill-Gibbs-Duhem equation (2.18) for the REV:

$$d(\widehat{p}V^{REV}) = SdT + pdV^{REV} + N_f d\mu_f + N_r d\mu_r. \tag{2.39}$$

Here the volume of the REV V^{REV} is that of the unit cell. When temperature T and volume of REV V^{REV} is constant, equation(2.39) reduces to:

$$d\widehat{p} = \frac{N_f}{V^{REV}}d\mu_f + \frac{N_r}{V^{REV}}d\mu_r = \rho_f d\mu_f + \rho_r d\mu_r. \tag{2.40}$$

We observe that two of the variables in equation(2.40) can be varied freely. The third variable follows when two are given. The situation here differs as we have the variable $\widehat{p}$ to deal with in comparison to bulk fluid, where we could compute the activity of the solvent once the activity of the solute is known. A change in the fluid chemical potential in the reservoir next to FCC unit cell will change the chemical potential μ of the solid particles in the porous medium.

Following the way we control the system, We postulate the following relation:

$$\frac{N_f}{V^{REV}}d\mu_f + \frac{N_r}{V^{REV}}d\mu_r = \frac{N_f}{V_f}d\mu_f. \tag{2.41}$$

It also shows that $d\widehat{p}$ is given by:

$$d\widehat{p} = \frac{N_f}{V_f}d\mu_f = \frac{\rho_f}{\phi}d\mu_f. \tag{2.42}$$

The system is in equilibrium, when the density of the fluids is the same as it is inside the FCC unit cell. We have equation(2.37) from earlier. Expanding the density term in terms of number of fluid particles N_f and fluid volume V_f, we get:

$$\widehat{p}(\mu) = \int \frac{N_f}{V_f} d\mu. \tag{2.43}$$

After applying equation(2.43) to the slit pore, and studying how well it describes the integral pressure $\widehat{p}$, we now try to expand upon it to apply it to the FCC unit cell by defining the unit cell as REV.

From equation(2.41), we get the following:

$$N_r d\mu_r = N_f (\frac{V^{REV}}{V_f} - 1) d\mu_f. \tag{2.44}$$

and the following:

$$\rho_r d\mu_r = \rho_f \frac{1-\phi}{\phi} d\mu_f. \tag{2.45}$$

Combining equations(2.41, 2.44 and 2.43) we get the following equation:

$$\widehat{p}(\mu) = \int \frac{N_f}{V^{REV}} + \frac{N_f (\frac{V^{REV} - V_r}{V_f})}{V^{REV}} d\mu. \tag{2.46}$$

Expressing the equation in terms of REV enables macro-scale description of the porous medium as disussed by Galteland et al [3].

Scaling Law

One way of studying pressure inside the porous medium is to use the microscopic pressure tensor [3, 7, 12]. When studying the integral pressure with the newly defined equation(2.46), we will use the pressure measurement provided by the pressure tensor as reference to compare our results against. In order to do this we can use scaling law.

At constant temperature T and chemical potential μ, we have the following:

$$d(\widehat{p} V^{REV}) = p dV^{REV}. \tag{2.47}$$

Rearranging it gives us:

$$p = \frac{d(\widehat{p} V^{REV}}{dV^{REV}} = \widehat{p} + V^{REV} \frac{d\widehat{p}}{dV^{REV}}. \tag{2.48}$$

We can then obtain a scaling law by computing the relation in equation(2.48) and plotting it vs the characteristic length or lattice constant a:

$$p - \widehat{p} = V^{REV} \frac{d\widehat{p}}{dV^{REV}} = \frac{\epsilon}{V^{REV}} = C \frac{\Omega^{REV}}{V^{REV}}. \tag{2.49}$$

Where and ϵ is the subdivision potential and Ω^{REV} is the surface of the FCC unit cell. Resulting in the ratio $\frac{\Omega^{REV}}{V^{REV}} = 6/a$ for a cubic unit cell.

Entropy Density of Confined Fluid

When the sizes of the FCC unit cell is constant, in other words the volume of the REV V^{REV}, and chemical potential μ is constant, equation(2.39) reduces to:

$$d(\widehat{p}V^{REV}) = SdT. \tag{2.50}$$

Equation(2.50) relates the variation in integral pressure $\widehat{p}$ to the entropy density by:

$$d(\widehat{p}) = \frac{S}{V^{REV}} dT. \tag{2.51}$$

Here S refers to the entropy of the unit cell.

Chapter 3

Methods

Molecular dynamic simulations of the slit pore and porous medium were carried out using the software LAMMPS [13]. The experiment was set up to use grand canonical Monte Carlo with molecular dynamics simulation using the Nosé-Hoover thermostat. This provided us with experiments with constant chemical potential μ, temperature T, volume V and surface area Ω.

3.1 Lennard-Jones spline

The Lennard-Jones (LJ) potential (V_{LJ}) is a model capable of describing many real systems. It is simple and particularly well suited for noble gases [14] or van der Waals systems in general. It is defined as follows:

$$V_{LJ} = 4\epsilon\left[\left(\frac{\sigma}{r}\right)^{12} - \left(\frac{\sigma}{r}\right)^{6}\right]. \tag{3.1}$$

In equation (3.1), the parameter ϵ describes the strength of the interaction and σ defines a length scale. The $\frac{1}{r^{12}}$ term describes Pauli repulsion at short ranges caused by overlapping electron orbitals. The $\frac{1}{r^{6}}$ term describes the attractive long-range, van der Waals, force. σ is defined as $r = \sigma$ when $V_{LJ} = 0$ (it actually passes through zero).

When used in computer simulations, the inter-molecular potential is truncated. The truncation typically happens at a distance of 2-5-5 molecular diameters. Although this truncation has little effect on the system@s structure, to fully represent Lennard-Jones system´s thermodynamic properties, the contributions from

the long-range tail must be included via tail corrections [14]. Properties such as surface tension and shift in potential, are sensitive to truncation. So one must take care in specifying how the potential is truncated and corrected.

Lennard-Jones spline (LJ/s) potential is an alternative to LJ potential. The LJ/s potential is a LJ potential truncated in such a way that it avoids the need for further specification. It eliminates the risk of ambiguity in how the potential is used in simulations. It essentially has the same structural features as the LJ potential model, but with different thermodynamic properties as the potential is of shorter range [14]. The pair potential of LJ/s is given by [14]:

$$V_{LJ/s} = \begin{cases} 4\epsilon\left[\left(\frac{\sigma}{r}\right)^{12} - \left(\frac{\sigma}{r}\right)^{6}\right] & \text{for } r < r_s, \\ a(r-r_c)^2 + b(r-r_c)^3 & \text{for } r_s < r < r_c, \\ 0 & \text{for } r > r_c. \end{cases} \tag{3.2}$$

Compared to equation (3.1, equation (3.2) has some additional parameters. The parameter r_s is the distance given by the LJ potential´s inflection point. Parameters $a, b,$ and r_c are defined so that the potential and its derivatives are continuous at r_s and r_c.

The short range of the LJ/s model leads to simulation times that are twice as fast in the liquid state in comparison with LJ model truncated at 2.5σ [14].

We use reduced units to work with simulations using LJ/s, this enables us to run simulations and get results that can be interpreted for other elements. See table(3.1) for a list of the reduced units we use.

3.2 Grand Canonical Monte Carlo

The principle idea of importance sampling is to use Monte Carlo procedure to generate random walk in regions of phase space with an important contribution to an ensemble average[15]. However, for my work we will be using a hybrid version of grand canonical Monte Carlo that only handles insertion and removal of particles, and not the displacement of particles. A basic equation for Monte Carlo simulations in the grand canonical ensemble is [15]:

$$\mathcal{N}_{\mu VT}(\boldsymbol{s}^N; N) \propto \frac{exp(\beta\mu N)V^N}{\bigwedge^{3N} N!} exp[-\beta\mathcal{U}(\boldsymbol{s}^N)]. \tag{3.3}$$

When it comes to grand canonical Monte Carlo simulation, we have to sample the distribution for instance using the equation (3.3). The following are the acceptable trial moves:

1. Displacement of particles: A particle is selected at random and given a new conformation. An example in the case of atoms could be random displacement. A displacement of particles is accepted with the following probability [15]:

$$acc(s \to s') = min(1, exp\{-\beta[\mathcal{U}(\boldsymbol{s'}^N) - \mathcal{U}(\boldsymbol{s}^N)]\}). \tag{3.4}$$

   Note that my work does not use this as it is a hybrid of grand canonical Monte Carlo and molecular dynamics. The simulation does not do displacement the way we set it up.
2. Insertion and removal of particles: A particle is created or inserted at a random position. Or the particle is randomly selected to be removed [15].
   The creation of a particle is accepted with the following probability [15]:

$$acc(N \to N+1) = min\left[1, \frac{V}{\bigwedge^3(N+1)} exp\{\beta[\mu - \mathcal{U}(N+1) + \mathcal{U}(N)]\}\right]. \tag{3.5}$$

   The removal of a particle is accepted with the following probability [15]:

$$acc(N \to N-1) = min\left[1, \frac{\bigwedge^3 N}{V} exp\{-\beta[\mu|\mathcal{U}(N1) + \mathcal{U}(N)]\}\right]. \tag{3.6}$$

3.3 Molecular Dynamics

Molecular dynamics is a technique used for computing equilibrium and transport properties of many-body system [15]. Many-body systems here refers to many-body system where the nuclear motion of the constituent particles obeys the laws of classical mechanics. We could therefore call it classical many-body system. This provides us with an excellent approximation for a wide range of materials. We need not worry about quantum effects unless we are to consider factors such as translational or rotational motion of light atoms or molecules such as: He, H_2, D_2 or vibrational frequency ν such that $h\nu > k_B T$ [15].

Molecular dynamics (MD) simulations is a way to conduct experimental work. The process by which one conducts simulation via MD is in many ways similar to

how real experiments work. We prepare a sample by selecting a model system consisting of N particles and solve Newton´s equations of motion for this system until the properties of the system no longer changes with time, i.e the system has reached equilibrium. When equilibrium has been reached, we perform measurements of our particular interest. Even the potential sources of error is in many ways similar between computer based MD experiments and real experiments. Some examples are errors such as samples not being prepared correctly, too short of measurement, system undergo irreversible change during experiment, or not measuring what we intended to measure [15].

We need to be able to express an observable quantity in terms of functions of the positions and momenta of the particles in the system, to be able to measure this observable quantity [15].

3.3.1 MD at Constant Temperature

MD simulations for this work were carried out at constant temperature. From a statistical mechanical perspective, we can impose a temperature on a system by bringing it into thermal contact with a large heat bath. Providing conditions under which the probability of finding the system at a given energy state is given by Boltzmann distribution [15].

We have a simple relation between the imposed temperature T and the kinetic or translational energy per particle [15]. When considering MD simulations, the condition of constant temperature is not equivalent to the condition that the kinetic energy per particle is constant. This is understandable when one considers the relative variance of the kinetic energy per particle in a canonical ensemble. Constraining kinetic energy to be always equal to its average leads to the variance vanishing by construction. In a canonical ensemble of finite system, the instantaneous kinetic temperature fluctuates [15]. We would in fact not be simulating the true constant-temperature ensemble if we were to keep the average kinetic energy per particle rigorously constant [15].

We use the Nosé-Hoover thermostat to achieve isothermal molecular dynamics simulation. This MD scheme allows one to perform deterministic MD at constant temperature. The Nosé-Hoover thermostat is based on the use of extended Lagrangian. Extended Lagrangian is a Lagrangian that contains additional, artificial coordinates and velocities [15].

3.4 The Slit Pore

To simulate the slit pore, a simulation box was configured, and the fluid inside the slit pore was configured to be Lennard-Jones/spline particles. The grand canonical Monte Carlo simulation would then take care of particle creation and the removal of these particles in the system. The walls of the slit pore were not made up of particles. These were essentially only meant to confine the particles, and have attractive and repulsive forces on the fluid particles. In other words, there would not be any heat transfer between the walls themselves or between the walls and particles. There would also be no attractive or repulsive forces between the walls, i.e no wall-wall interaction.

Working with Lennard-Jones particles, it becomes convenient to use dimensionless units or reduced units, here refered to as Lennard-Jones units. Description of these units can be found in table (3.1)[11].

Table 3.1: The reduced units are denoted with an asterisk in superscript. The variables are reduced using the molecular diameter of the fluid σ, potential well depth ϵ, fluid particle mass m and Boltzmann constant k_B

Description	**Definition 3**
Energy	$E^* = E/\epsilon$
Entropy	$S^* = S/k_B$
Temperature	$T^* = Tk_B/\epsilon$
Distance	$x^* = x/\sigma$
Pressure	$p^* = p\sigma^3/\epsilon$
Chemical Potential	$\mu^* = \mu/\epsilon$

Two sets of experiments were run and then processed with LAMMPS and in-house software to calculate the local mechanical pressure tensor.

3.4.1 Constant height, varying chemical potential

For this set of experiments, the slit pore was configured to have a constant temperature of 2 in reduced units using the Nosé-Hoover thermostat. The simulation box would have lengths of 50 in z- and y-direction. Height of 4, i.e x-direction

of the simulation box. The variable to be studied with these experiments was the chemical potential μ. So, while keeping all the earlier mentioned variables constant, multiple experiments were run with varying chemical potential μ. Varying from -10 to 10.

3.4.2 Varying height, constant chemical potential

Unlike the previous experiment set, here we wished to study the system under varying height, and thus effectively volume. The slit pore was configured to have a constant temperature of 2 using the Nosé-Hoover thermostat. While the chemical potential μ in experiment set 1 varied, here the chemical potential was held constant at $\mu = 0$ The simulation box would have lengths of 50 in z- and y-direction, while the height, x-direction, would vary from 0.5 to 10.

3.5 Porous Medium

Once the simulations with slit pores were dealt with, and a better understanding of the nanothermodynamic framework was developed, we delved into applying the nanothermodynamic framework to a porous medium. The porous medium we set up was a FCC lattice unit cell, an example is illustrated in figure(3.1). It would have varying properties so that we could study it in different ways. As with the slit pore, the wall were not made up of particles, but rather just a confinement for the fluid particles that would be introduced to the system. The unit set is then defined as the REV by choice. In the figures presented in this paper, the blue particles will represent the solid particles of the FCC unit cell. The red particles will be representing the fluid particles. Denoted r and f respectively as it has been done in prior work by Galteland et al[3]. The units used here are also defined as they were for the slit pore, found in table 3.1. The wish was to study how temperature T, lattice constant a and thereby volume V, chemical potential μ would affect the system. Also comparisons between bulk and porous medium were conducted.

From figure(3.1) we see the property d illustrated. This is the distance between the closest solid particles. From previous work [3], it has been observed that for d greater than 11σ, σ being the diameter of the fluid particles, one could ignore contribution from disjoining pressure. So for the series of simulations run, we choose lattice constants a that can show this. i.e ensembles where d is slightly

above 11σ and down, but above 4σ.

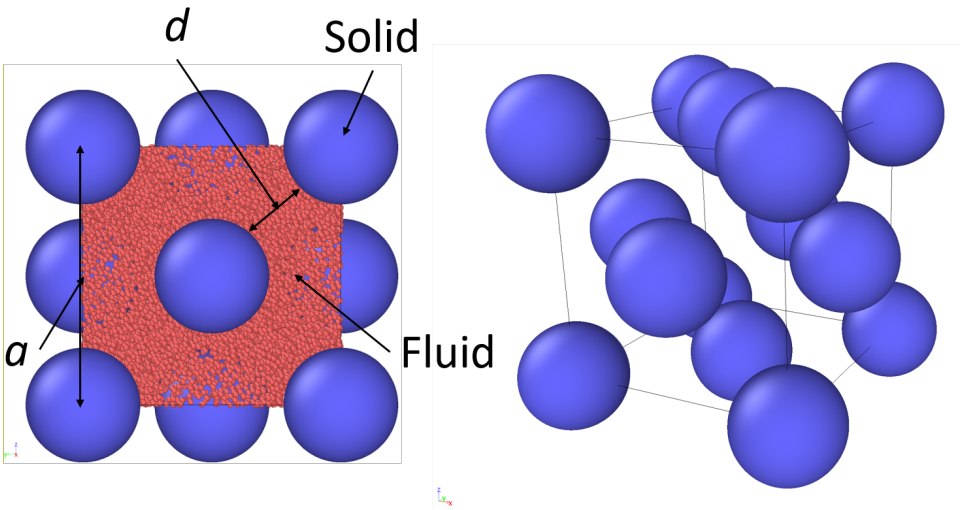

Figure 3.1: Diagram and visualization of the FCC unit cell. The red particles being the fluid particles, and the blue particles being the solid particles. Software used for rendering this figure is OVITO [16]

3.5.1 Lattice constant $a = 45$, $r = 10\sigma$

We set the lattice constant to $a = 45$ and radius of the solid particles to $r = 10\sigma$. This ensures that d is larger than 11, or more specifically $d = 11.820$. Simulations were run for FCC unit cell, and Bulk. Simulations were also done across temperatures $T = 1.0, 1.5, 2.0$

3.5.2 Lattice constant $a = 20, 25, 30.$ $r = 5\sigma$

To be able to compare with previous work and reference values from others working related topic, we ran simulations using solid particle radius 5σ. The chosen lattice constants are $a = 20, 25, 30$. The corresponding values of d are: $d = 4.142, 7.678, 11.213$ calculated using the following equation:

$$d = \frac{\sqrt{2a^2} - 4r}{2}. \tag{3.7}$$

Chapter 4

Results and Discussion

First I will present the results from the slit pore simulations. The aim being to see how well the nanothermodynamic description of the integral pressure fits with results gained from simulations. I then expand upon the new equation 2.37 to apply it to a porous medium, by factoring in REV. Results from simulations regarding the porous medium is presented after the slit pore section.

4.1 Slit Pore

The results are illustrated in figures 4.1 to 4.10. I will discuss the results in the order that they appear.

More than 100 simulations were run in order to collect the necessary data for this work. Figure (4.1) illustrates a rendition of such a simulation.

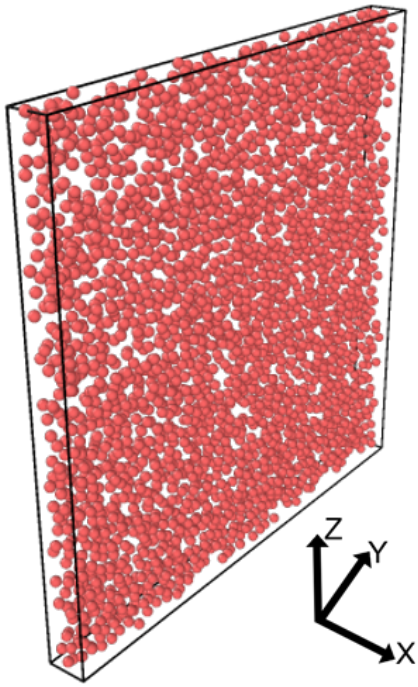

Figure 4.1: Visualization of the fluid particles in a slit pore of height = 4σ (x-direction), chemical potential $\mu^* = 0$, temperature $T^* = 2$. The solid lines illustrate the simulation box. Software used for rendering is OVITO [16].

The red balls in figure (4.1) represent the particles in the fluid phase. The solid lines represents a box that simulates a slit pore. Note that the height is defined in the x-direction, leaving y- and z-direction with large lengths. This implies that the change in volume to the system stems from the change in height alone, as there is no change in surface area of the walls.

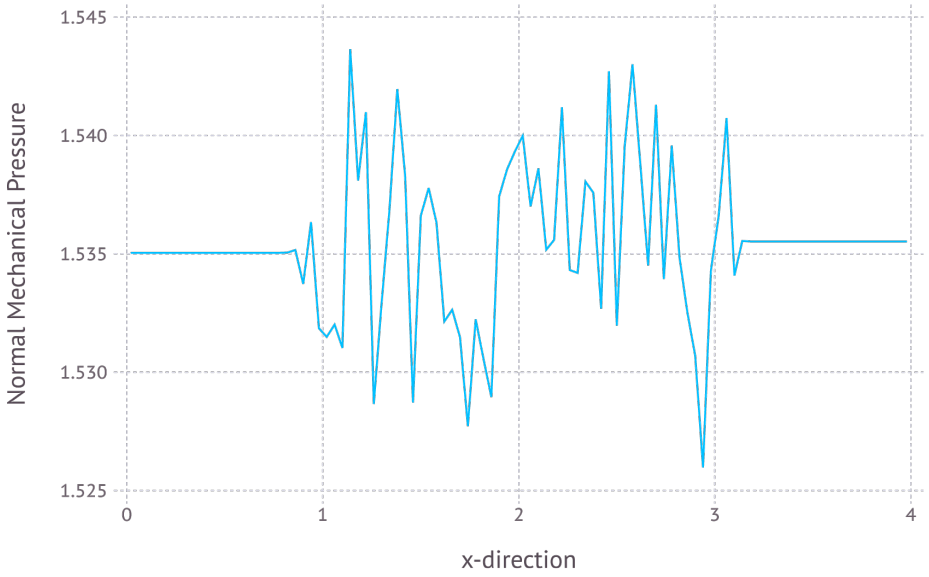

Figure 4.2: Illustrates the normal mechanical pressure for a slit pore with height $= 4\sigma$ (x-direction), chemical potential $\mu^* = 0$, temperature $T^* = 2$. Note that the scale on y-axis shows huge variation for small numbers. The graph shows how the normal mechanical pressure varies along the x-direction.

In figure (4.2) one can observe how the normal mechanical pressure varies along the x-direction of a simulated slit pore or simulation box. In all of the simulations the temperature was set to $T^* = 2.0$. While in this particular example the height was set to $h = 4.0\sigma$ and chemical potential to $\mu^* = 0$

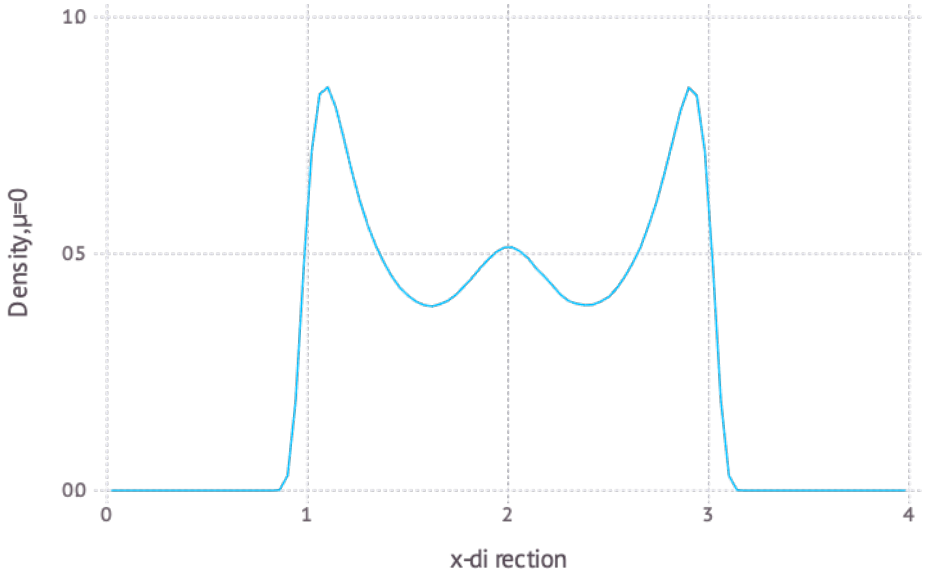

Figure 4.3: Illustrates the fluid number density ρ as a function of x-direction for a slit pore with height $= 4\sigma$ (x-direction), chemical potential $\mu^* = 0$, temperature $T^* = 2$. The graph shows how the density ρ varies along the x-direction.

Figure (4.3) shows the fluid number density data collected from the same example as those in figure (4.1) and figure (4.2). The three tops suggest the particles organizing in layers and keeps a certain distance from the walls at $x = 0$ and $x = 4$.

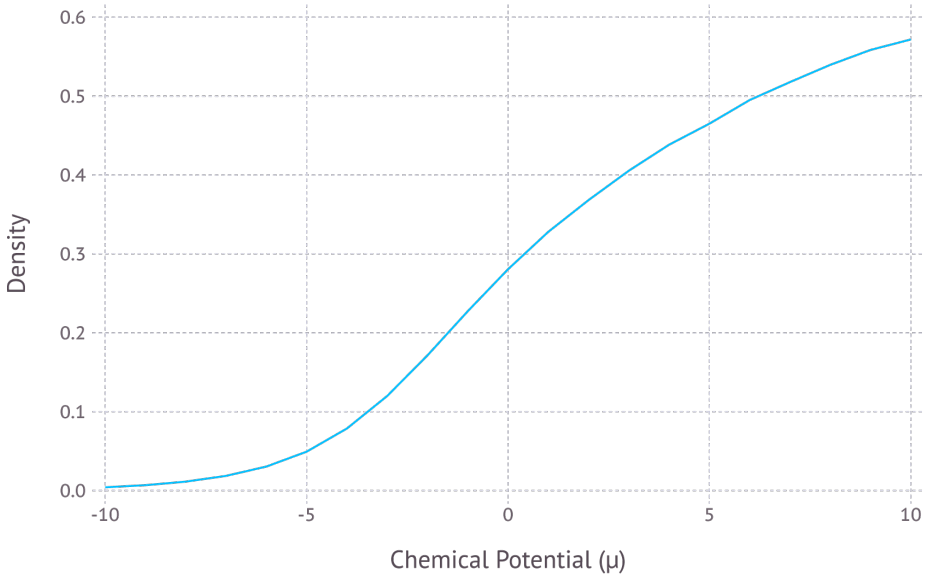

Figure 4.4: Illustrates the fluid number density ρ as a function of chemical potential μ for a slit pore with height $= 4\sigma$, temperature $T^* = 2$. The graph shows density profile of slit pores with varying chemical potential, keeping other properties constant.

Several simulations were run with varying chemical potential, while keeping other parameters constant. This allowed the study of how the nanothermodynamic description of a slit pore changes with varying chemical potential μ. Figure (4.4) presents a change in density as a function of chemical potential μ. It can be observed that the density goes towards zero as one goes lower than $\mu = -10$ and the density plateaus at a certain point, at which point one simply can not insert more particles into the defined system. Also, there is the case of the fluid particle eventually changing phase.

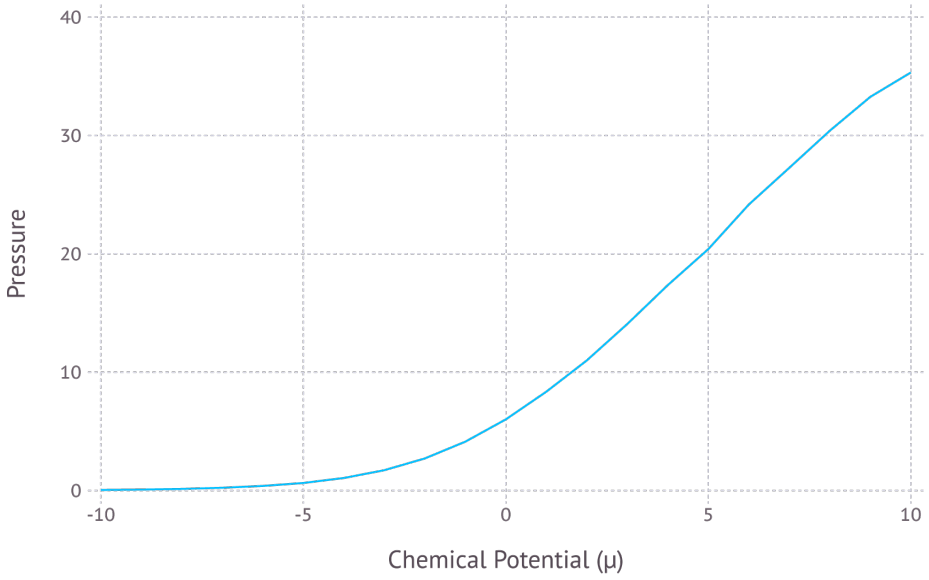

Figure 4.5: Illustrates the normal mechanical pressure ρ as a function of chemical potential μ for a slit pore with height $= 4\sigma$, temperature $T^* = 2$. The graph shows normal mechanical pressure profile of slit pores with varying chemical potential, keeping other properties constant.

Also normal mechanical pressure data was collected from the simulations run with varying chemical potential μ. It was observed that the normal mechanical pressure goes to zero as chemical potential gets smaller. It also seemed like the pressure had a tendency to taper off as the chemical potential started going above 10. This could indicate a change in conformation. As the particles start organizing more, at some point the fluid would start changing phase. Thus, getting more stable pressure despite higher chemical potential.

The second set of simulations held the chemical potential constant at $\mu = 0$, while the height h was varied.

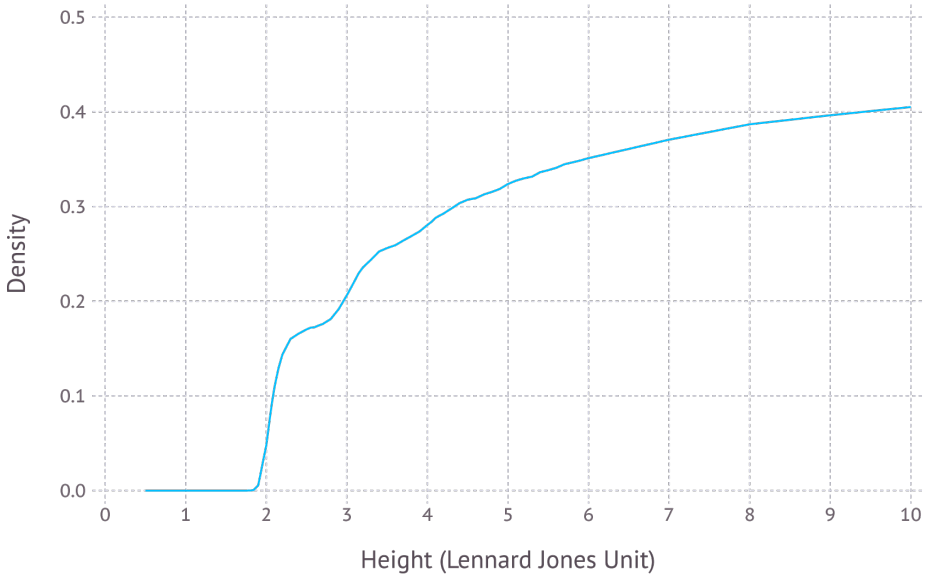

Figure 4.6: Illustrates the fluid number density ρ as a function of height for a slit pore with chemical potential $\mu = 0$, temperature $T^* = 2$. The graph shows density profile of slit pores with varying slit pore height, keeping other properties, including chemical potential, constant.

A density profile was created from data collected from the second set of simulations. This was the fluid number density defined as $\rho = N/V$.Figure (4.6) presents this density profile. By studying it we see that up till a certain point, the simulation was not able to insert particles into the system, thus the density till that point remains zero. The density then start plateauing as height increases.

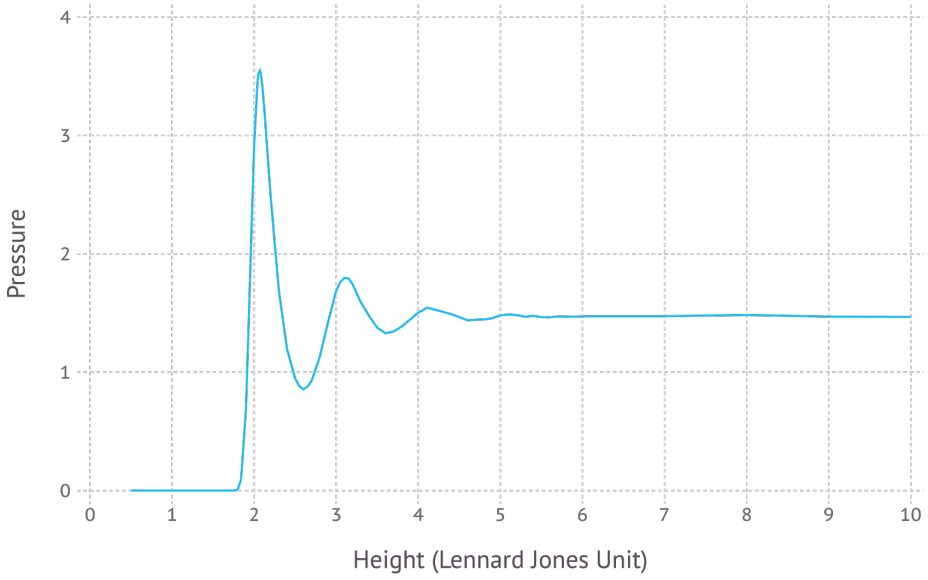

Figure 4.7: Illustrates normal pressure $P_\perp$ as a function of height for slit pores with chemical potential $\mu = 0$, temperature $T^* = 2$. The graph shows normal pressure profile of slit pores with varying slit pore height, keeping other properties, including chemical potential, constant.

I used equation (2.33) to present the data in figure (4.7). Where the normal pressure as a function height h is computed as the normal mechanical pressure component. The tops and minimums suggest a change in arrangement of the particles with varying height. In the beginning the box is so small the particles are likely more densely packed, as the height increases more efficient conformations are allowed, perhaps by allowing more layers of particles. Then the pressure builds up again till the height has increased enough to allow yet another more efficient conformation. This seems to continue till it at one point does not change significantly with increasing height.

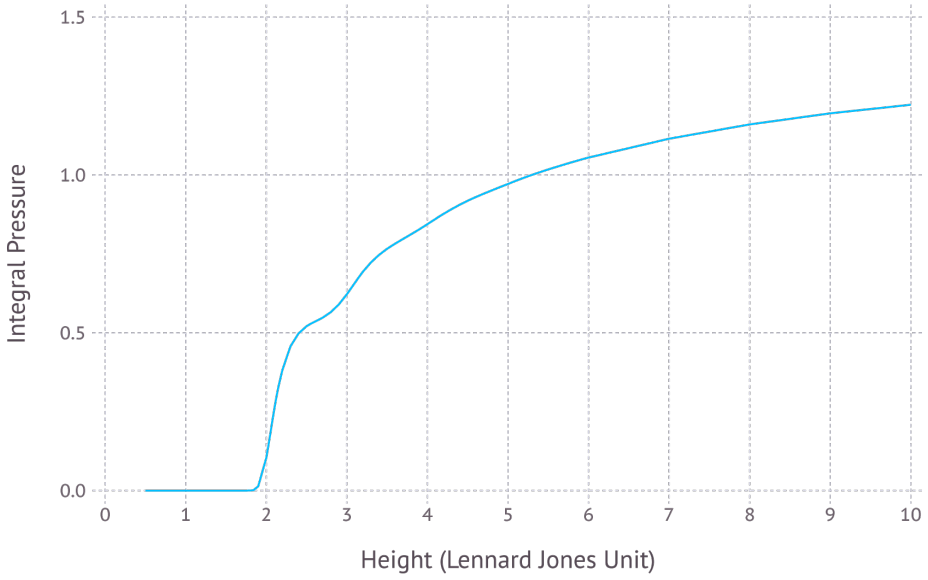

Figure 4.8: Illustrates integral pressure $\widehat{p}$ as a function of height for slit pores with chemical potential $\mu = 0$, temperature $T^* = 2$. The graph shows integral pressure profile of slit pores with varying slit pore height, keeping other properties, including chemical potential, constant.

From equation (2.33) we also get that $\widehat{p}(h) = \frac{1}{h}\int_0^h P_\perp dh$. I used this to evaluate the integral pressure as a function of slit pore height h. This can be seen in figure (4.8).

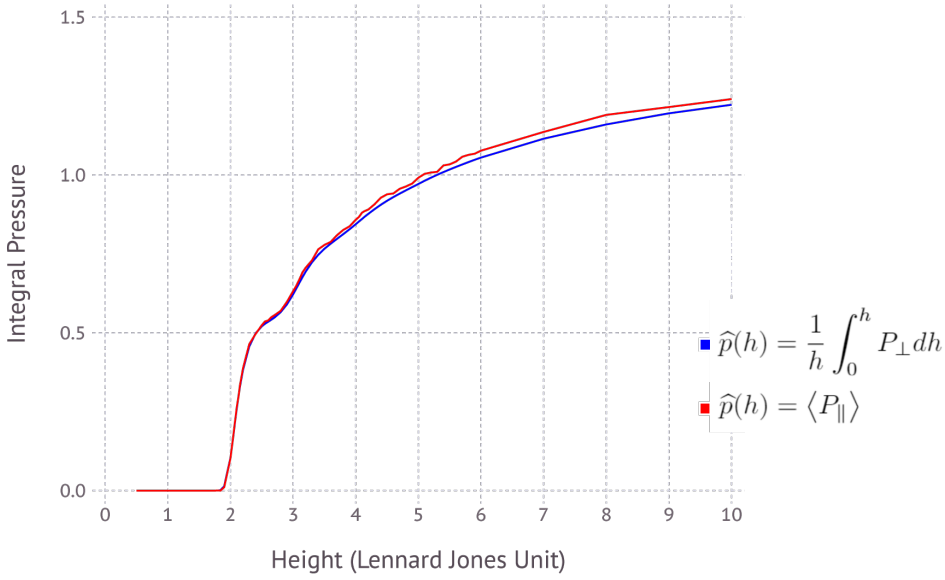

Figure 4.9: Compares integral pressure $\widehat{p}$ as a function of height for slit pores with chemical potential $\mu = 0$, temperature $T^* = 2$. The graph shows integral pressure profile obtained through normal pressure $P_\perp$(blue) and tangential pressure $P_\parallel$(red).

From equation (2.35) we also have that $\widehat{p}(h) = \langle P_\parallel \rangle$. Using this I compared the results of integral pressure as a funciton of height h calculated from normal mechanical pressure tensor with the results of integral pressure from tangential pressure. The graph where these two have been plotted can be found in figure (4.9). It can be observed that the results are matching, suggesting that the nanothermodynamic description of the integral pressure as a function of height matches regardless of pathway one takes to find it.

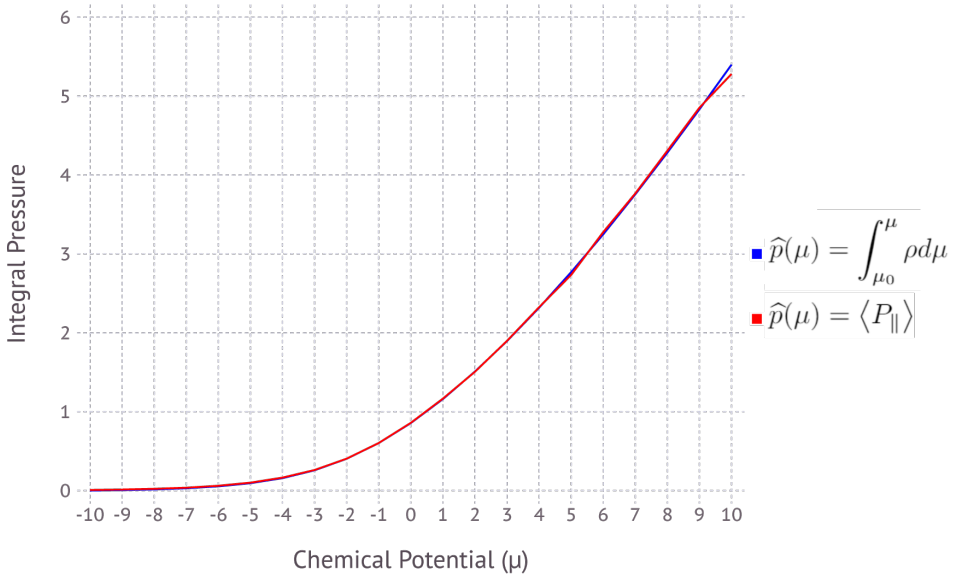

Figure 4.10: Compares integral pressure $\widehat{p}$ as a function of chemical potential μ for slit pores with height $= 4$, temperature $T^* = 2$. The graph shows integral pressure profile obtained from density ρ(blue) and tangential pressure $P_{\parallel}$(red).

The integral pressure as a function of chemical potential was evaluated by using equation (2.37). The results then got plotted against integral pressure as a function of chemical potential, based on the tangential pressure. To do this one can derive an equation from equation (2.35) to consider it as a function of chemical potential rather than height. Figure (4.10) present the comparison of these two plots. One can observe that the nanothermodynamic description of the integral pressure of slit pores as function of chemical potential μ yields similar results by studying the figure(4.11), whether it is evaluated via the density or the tangential pressure. Especially for chemical potential μ values below 10.

It is essentially shown that $\widehat{p} = \frac{-X}{V} = \frac{1}{h} \int P_{\parallel} dx$.

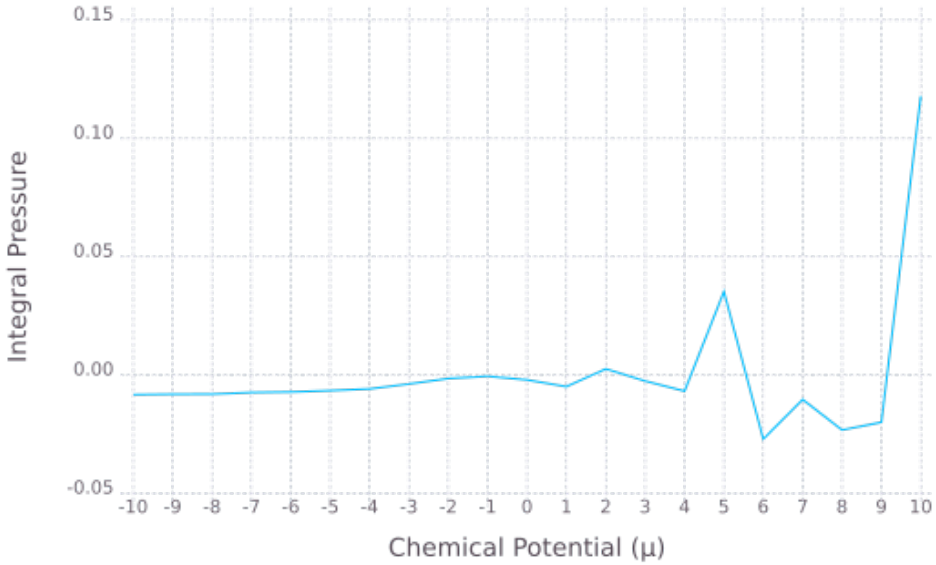

Figure 4.11: Shows the difference between the integral pressure values obtained from density ρ and tangential pressure $P_{\|}$ for the values show in figure(4.10)

.

4.2 Porous Medium

4.2.1 lattice constant $a = 45$

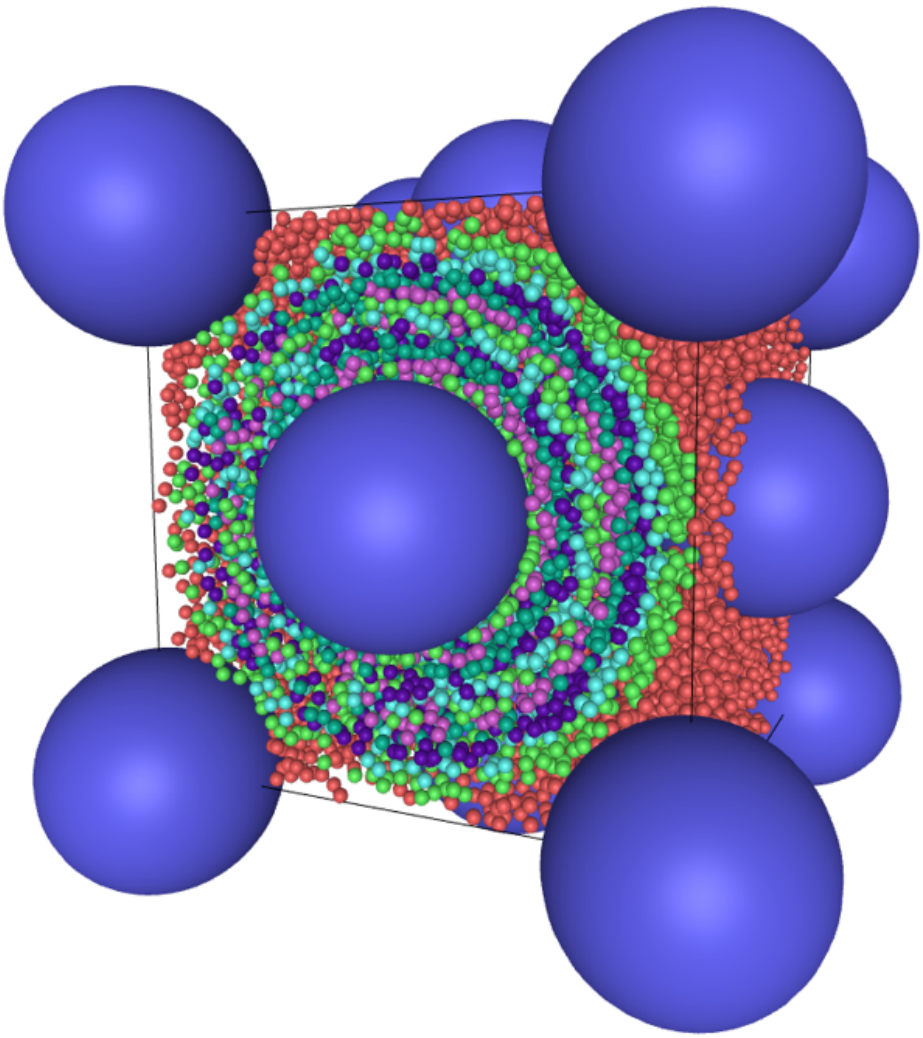

Figure 4.12: Diagram and visualization of the FCC unit cell. The red particles being the fluid particles, and the blue particles being the solid particles. The rainbow colored particles being organized in shells around a specific solid particle with increasing distance. Software used for rendering was made in-house

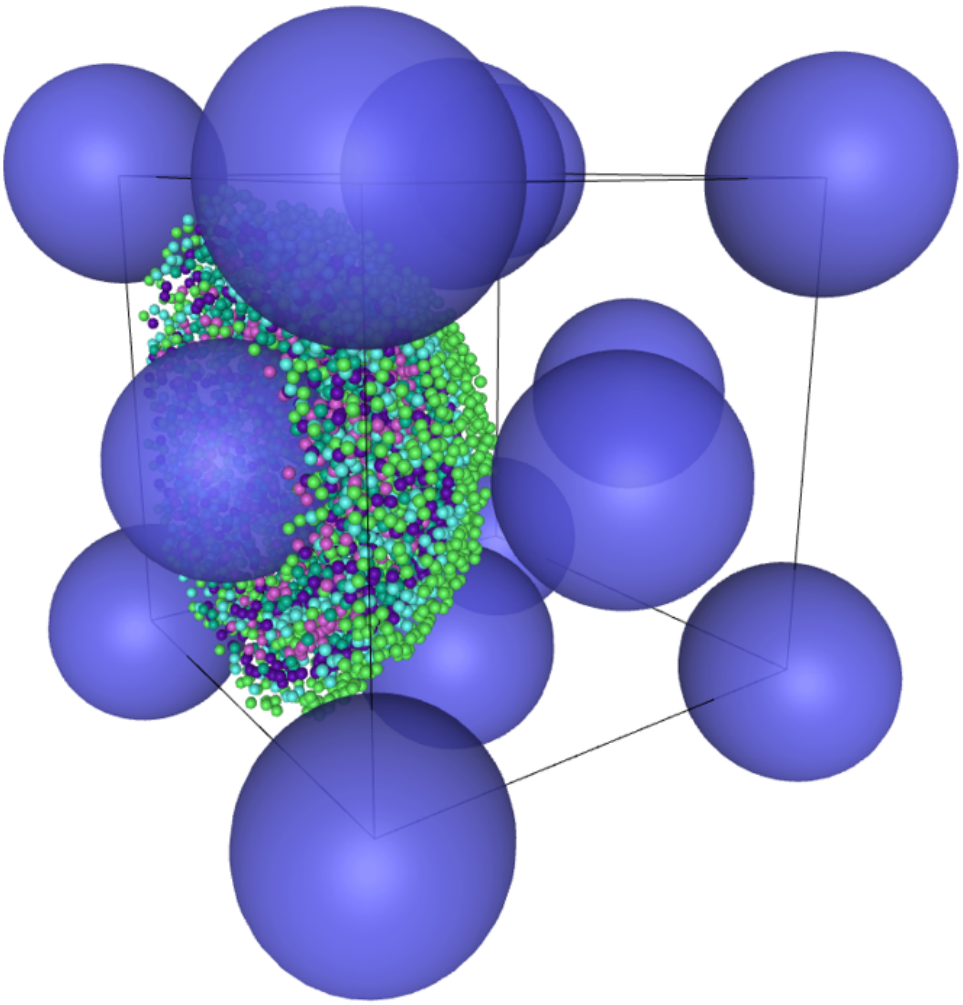

Figure 4.13: Diagram and visualization of the FCC unit cell. The blue particles being the solid particles. The rainbow colored particles being organized in shells around a specific solid particle with increasing distance. Software used for rendering was made in-house

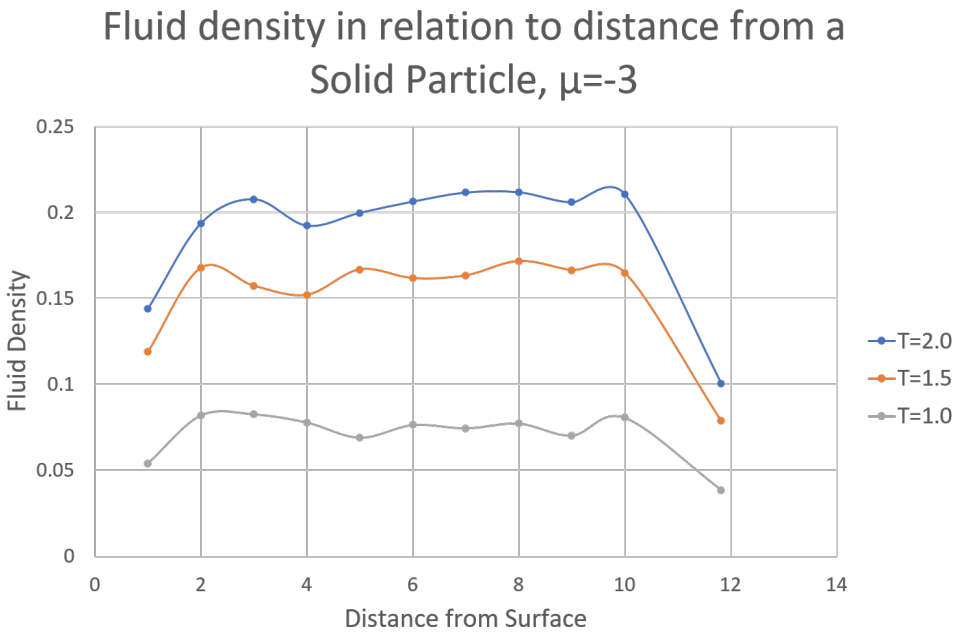

Figure 4.14: Figure showing the fluid density from one particle to the next. Se figure(4.12) to visualize how the density was computed. For FCC unit cell with lattice constant $a = 45$. At equilibrium when chemical potential $\mu = -3$. For different temperatures.

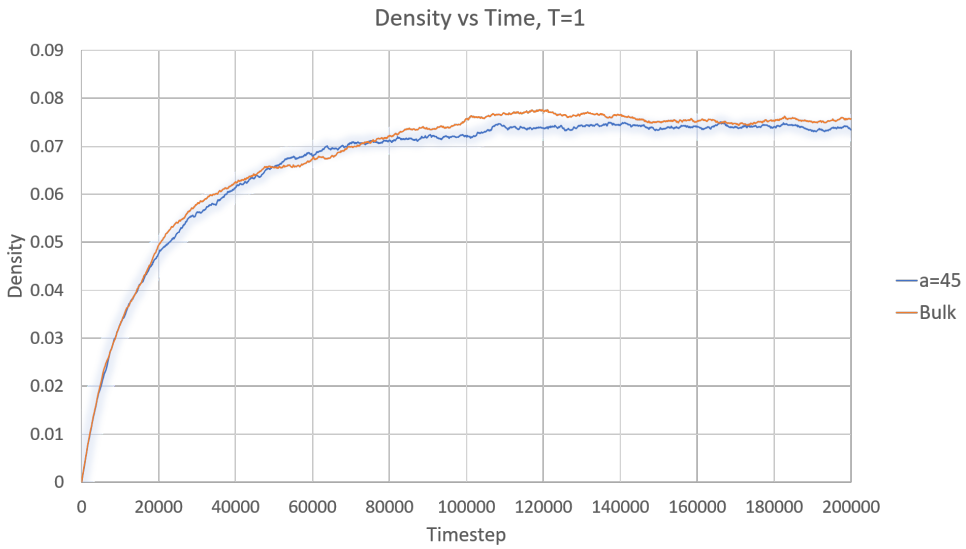

Figure 4.15: Fluid density as a function of time. lattice constant $a = 45$. Chemical potential $\mu = -3$. Comparison between FCC unit cell(blue) and Bulk(red) of same unit volume. Temperature $T = 1.0$

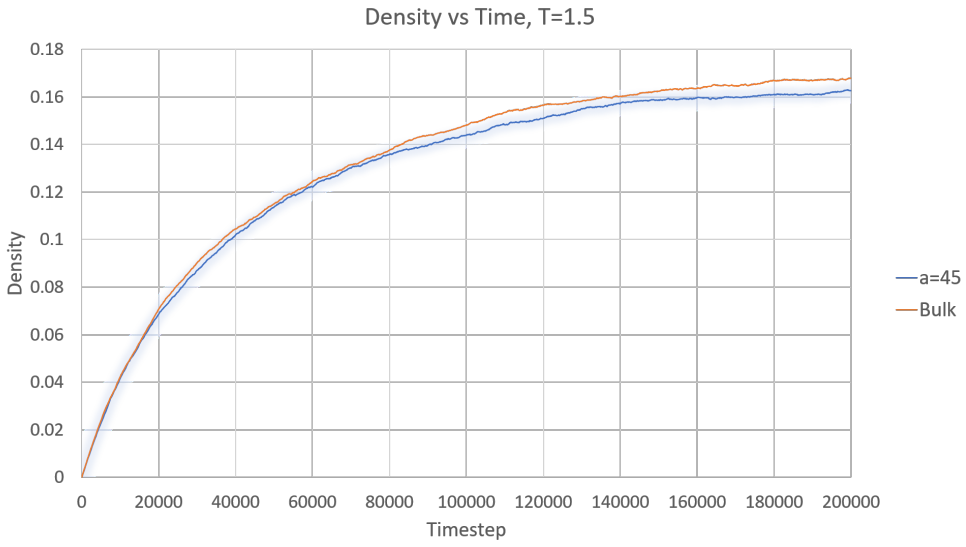

Figure 4.16: Fluid density as a function of time. lattice constant $a = 45$. Chemical potential $\mu = -3$. Comparison between FCC unit cell(blue) and Bulk(red) of same unit volume. Temperature $T = 1.5$

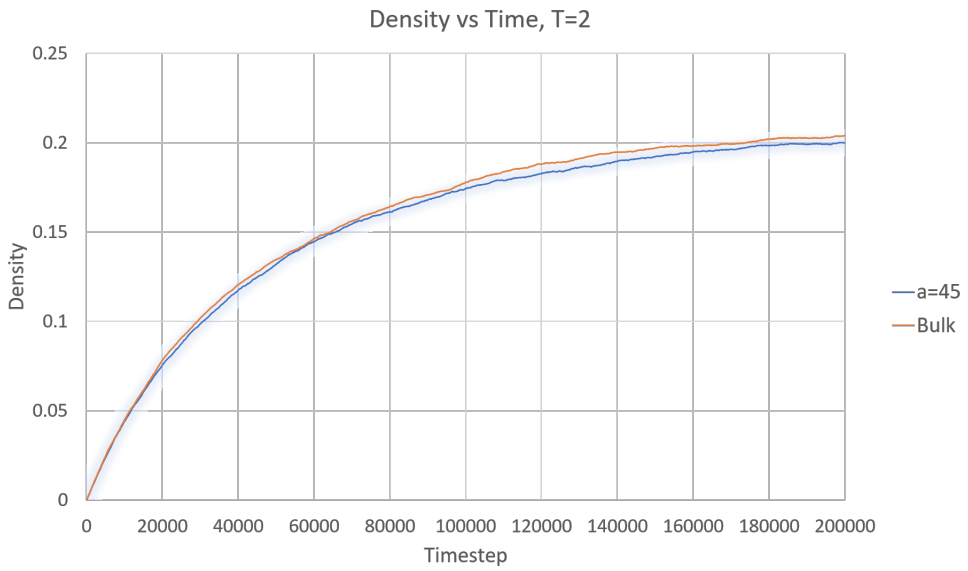

Figure 4.17: Fluid density as a function of time. lattice constant $a = 45$. Chemical potential $\mu = -3$. Comparison between FCC unit cell(blue) and Bulk(red) of same unit volume. Temperature $T = 2.0$

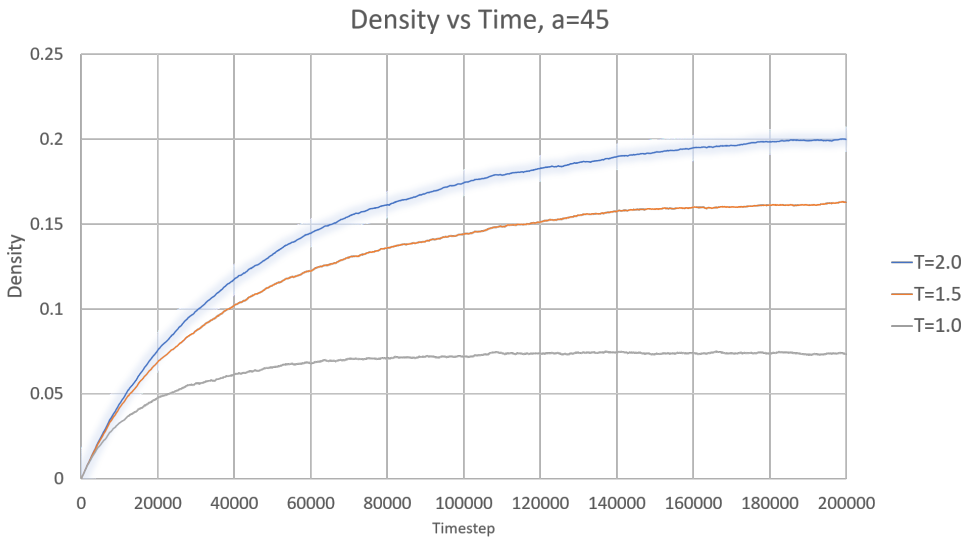

Figure 4.18: Fluid density as a function of time. lattice constant $a = 45$. Chemical potential $\mu = -3$. Comparison between different temperatures $T = 1.0, 1.5, 2.0$.

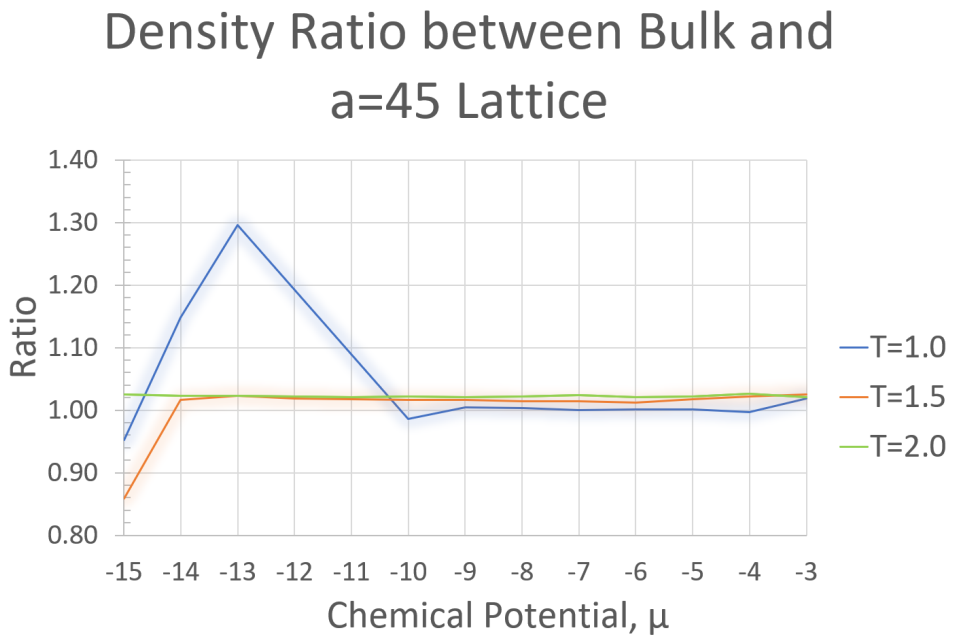

Figure 4.19: Ratio between Bulk and FCC unit cell with lattice constant $a = 45$. As a function of Chemical potential μ. For different temperatures $T = 1.0, 1.5, 2.0$.

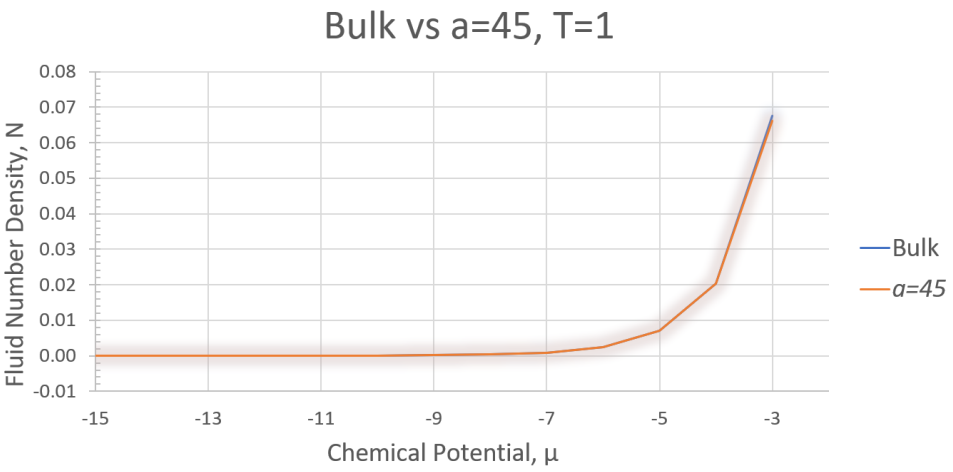

Figure 4.20: Comparison of Fluid Number density N as a function of chemical potential μ for FCC unit cell vs Bulk. At temperature $T = 1.0$

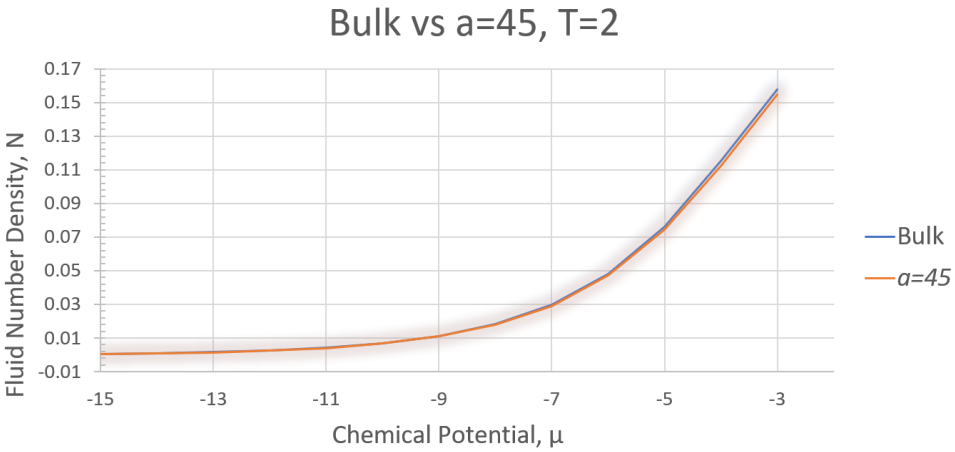

Figure 4.21: Comparison of Fluid Number density N as a function of chemical potential μ for FCC unit cell vs Bulk. At temperature $T = 2.0$

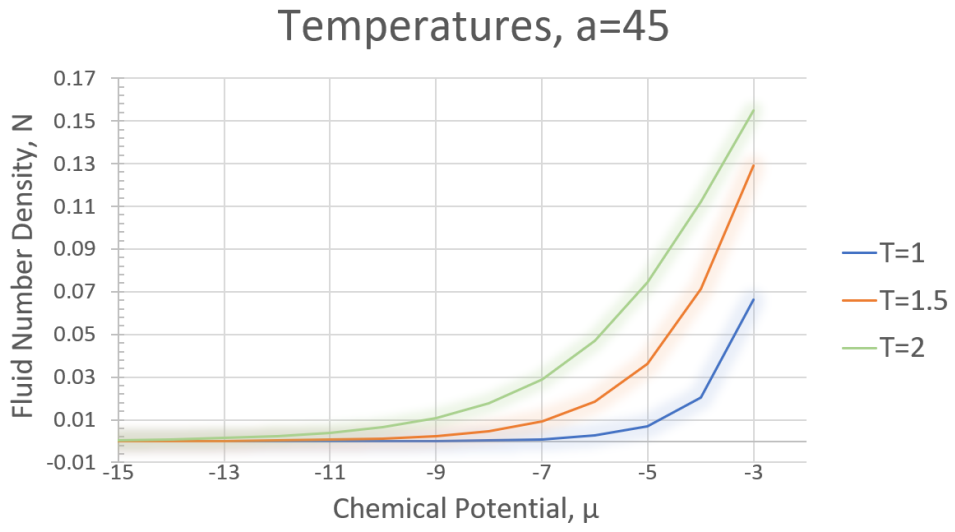

Figure 4.22: Fluid number density N as a function of chemical potential μ for FCC lattice unit cell with $a = 45$ at different temperatures $T = 1.0, 1.5, 2.0$

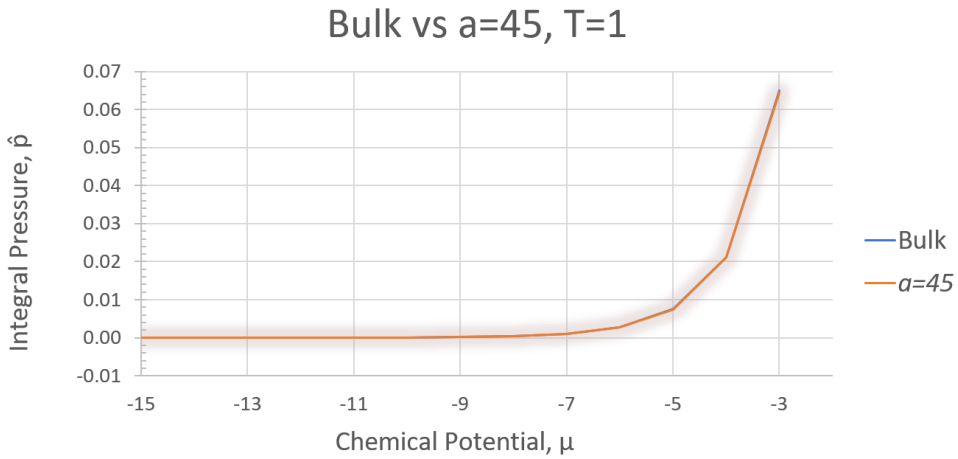

Figure 4.23: Comparison of Integral pressure $\widehat{p}$ as a function of chemical potential μ for FCC unit cell(orange) with lattice constant $a = 45$ and Bulk(blue). At temperature $T = 1.0$

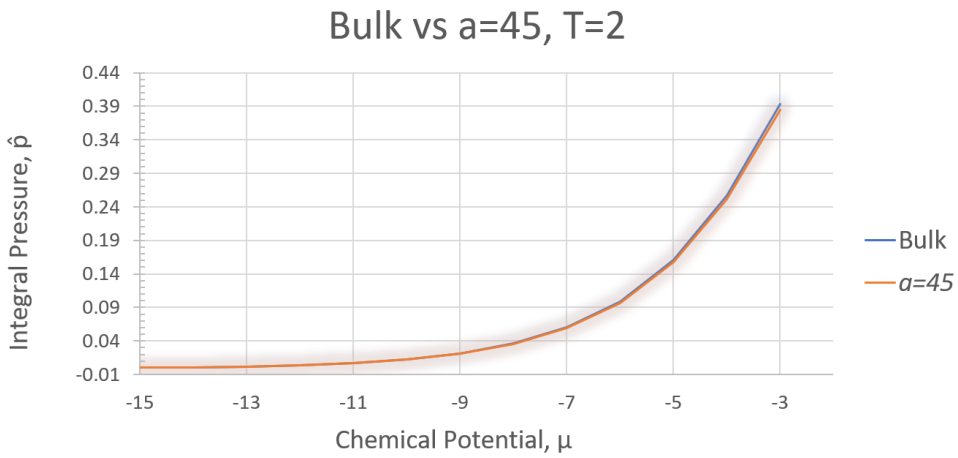

Figure 4.24: Comparison of Integral pressure $\widehat{p}$ as a function of chemical potential μ for FCC unit cell(orange) with lattice constant $a = 45$ and Bulk(blue). At temperature $T = 2.0$

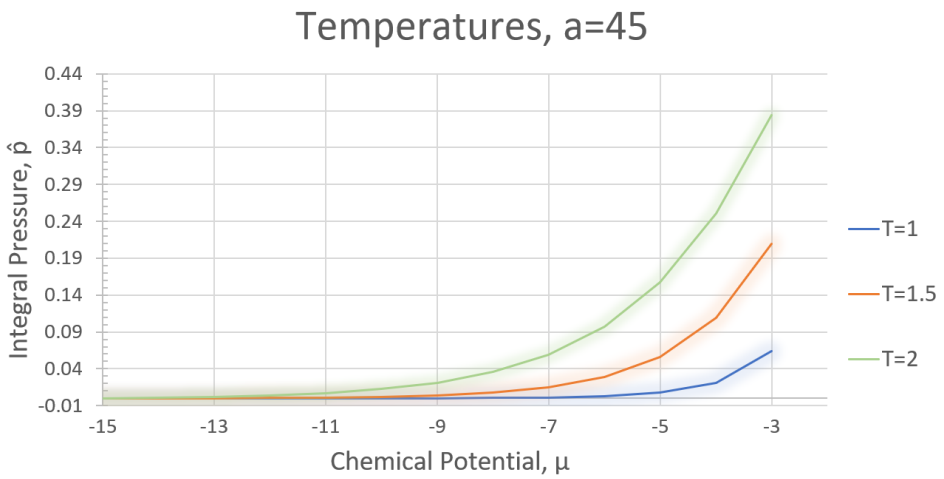

Figure 4.25: Integral pressure $\widehat{p}$ as a function of chemical potential μ for FCC unit cell with lattice constant $a = 45$ at different temperatures $T = 1.0, 1.5, 2.0$

4.2.2 Lattice constant $a = 20, 25, 30.$ $r = 5\sigma$

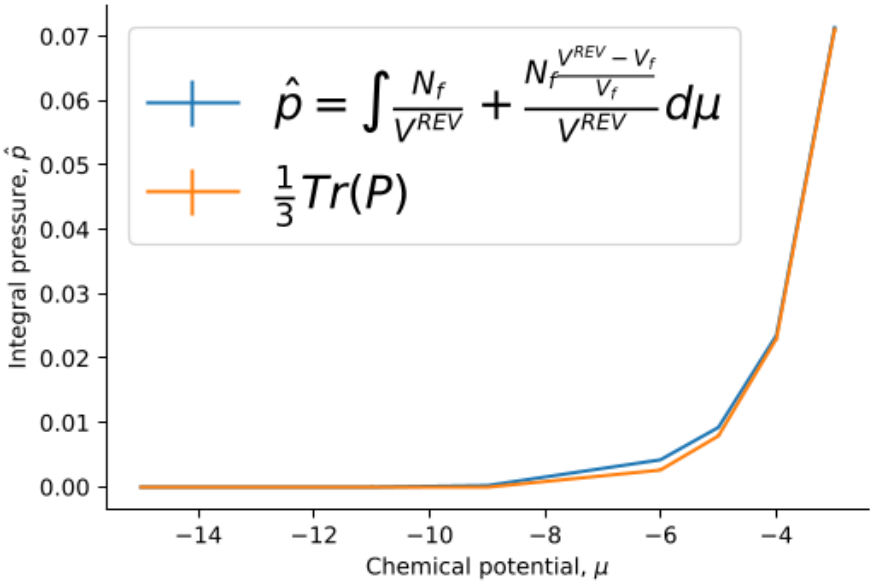

Figure 4.26: Integral pressure $\widehat{p}$ computed using the new method, equation(2.46) and Trace of pressure tensor. For $a = 20$ and temperature $t = 1.0$

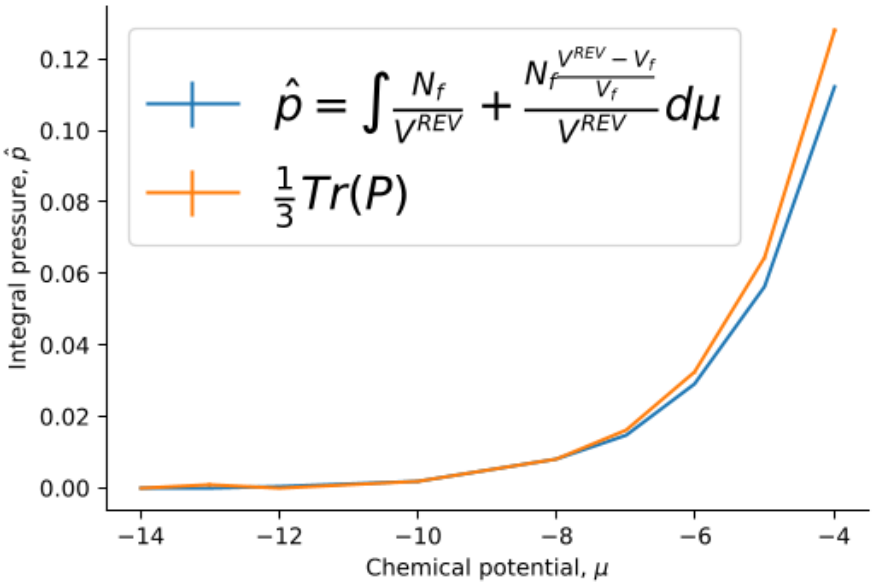

Figure 4.27: Integral pressure $\widehat{p}$ computed using the new method, equation(2.46) and Trace of pressure tensor. For $a = 20$ and temperature $t = 1.5$

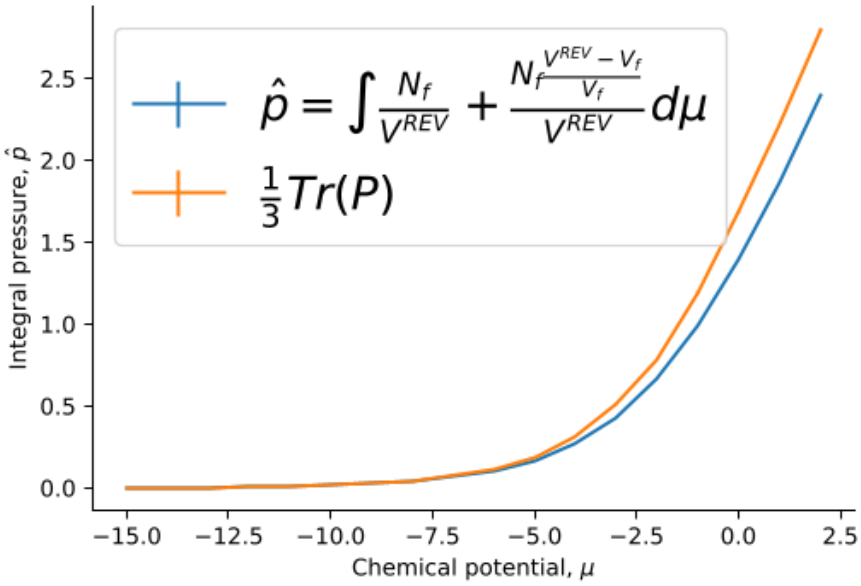

Figure 4.28: Integral pressure $\widehat{p}$ computed using the new method, equation(2.46) and Trace of pressure tensor. For $a = 20$ and temperature $t = 2.0$

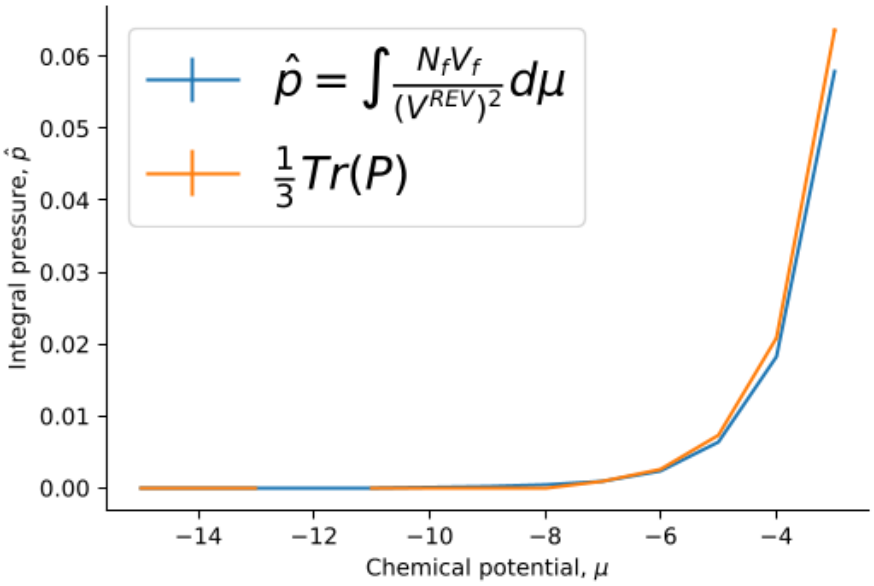

Figure 4.29: Integral pressure $\widehat{p}$ computed using the new method, equation(2.46) and Trace of pressure tensor. For $a = 25$ and temperature $t = 1.0$

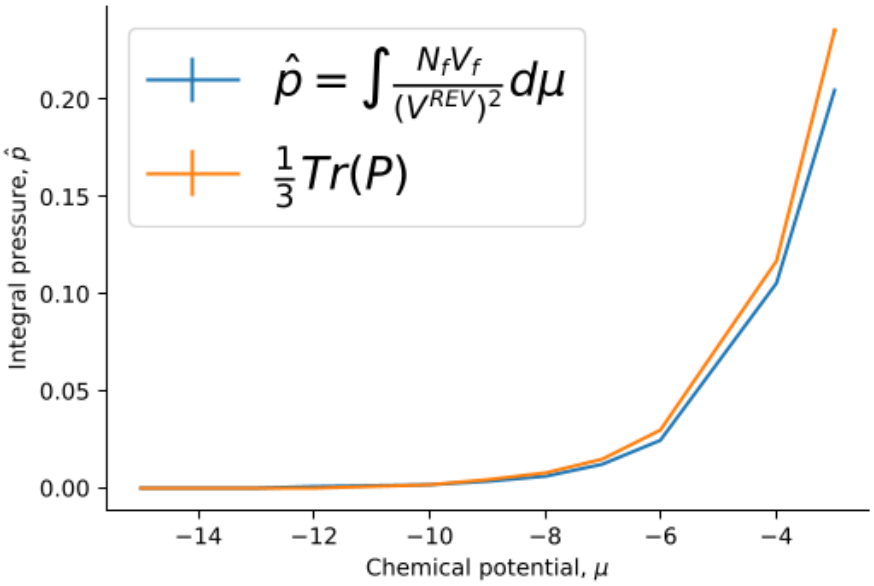

Figure 4.30: Integral pressure $\widehat{p}$ computed using the new method, equation(2.46) and Trace of pressure tensor. For $a = 25$ and temperature $t = 1.5$

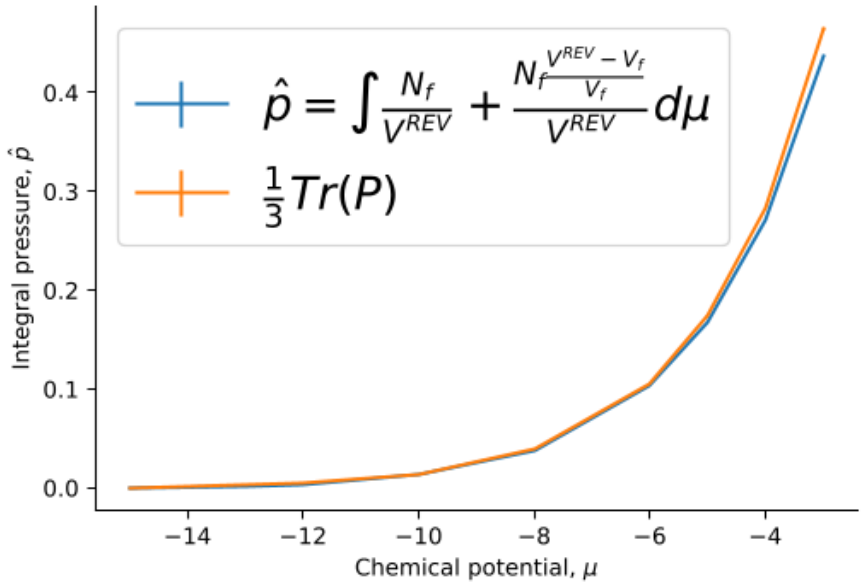

Figure 4.31: Integral pressure $\widehat{p}$ computed using the new method, equation(2.46) and Trace of pressure tensor. For $a = 25$ and temperature $t = 2.0$

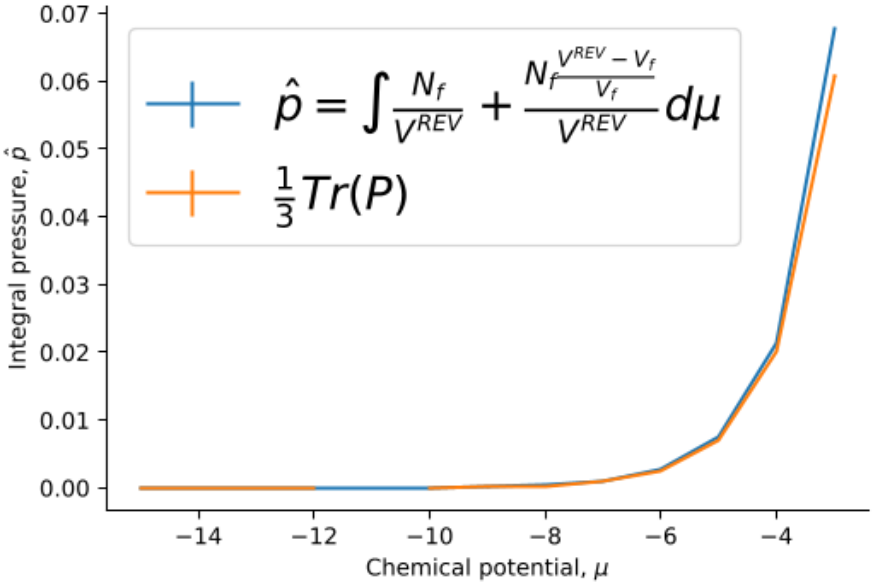

Figure 4.32: Integral pressure $\widehat{p}$ computed using the new method, equation(2.46) and Trace of pressure tensor. For $a = 30$ and temperature $t = 1.0$

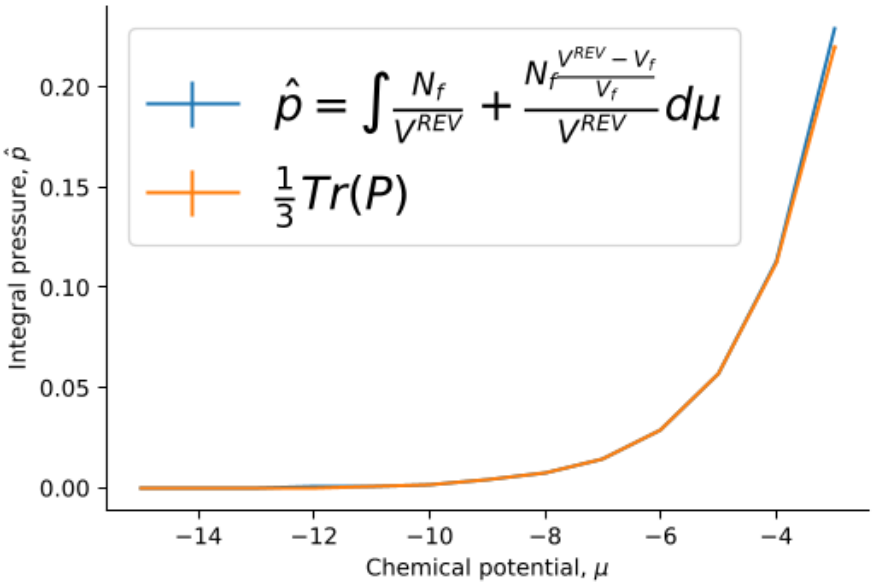

Figure 4.33: Integral pressure $\widehat{p}$ computed using the new method, equation(2.46) and Trace of pressure tensor. For $a = 30$ and temperature $t = 1.5$

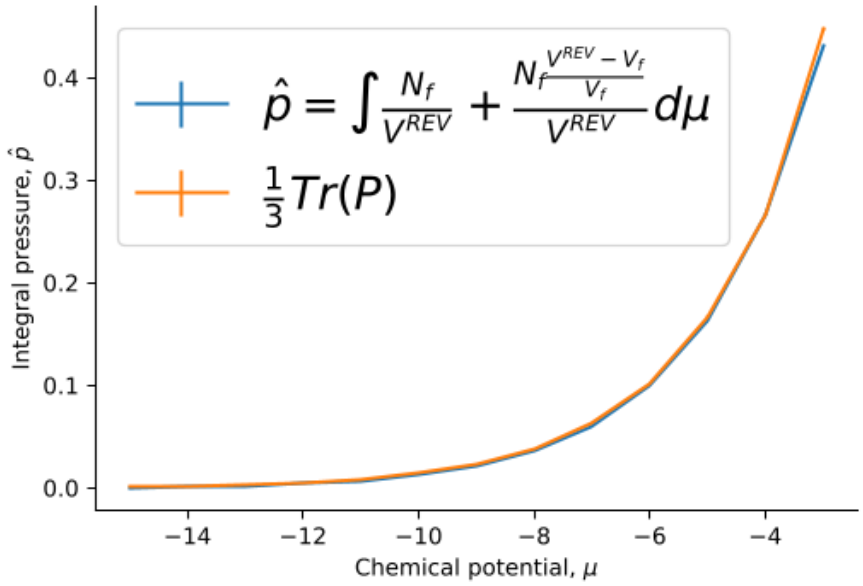

Figure 4.34: Integral pressure $\widehat{p}$ computed using the new method, equation(2.46) and Trace of pressure tensor. For $a = 30$ and temperature $t = 2.0$

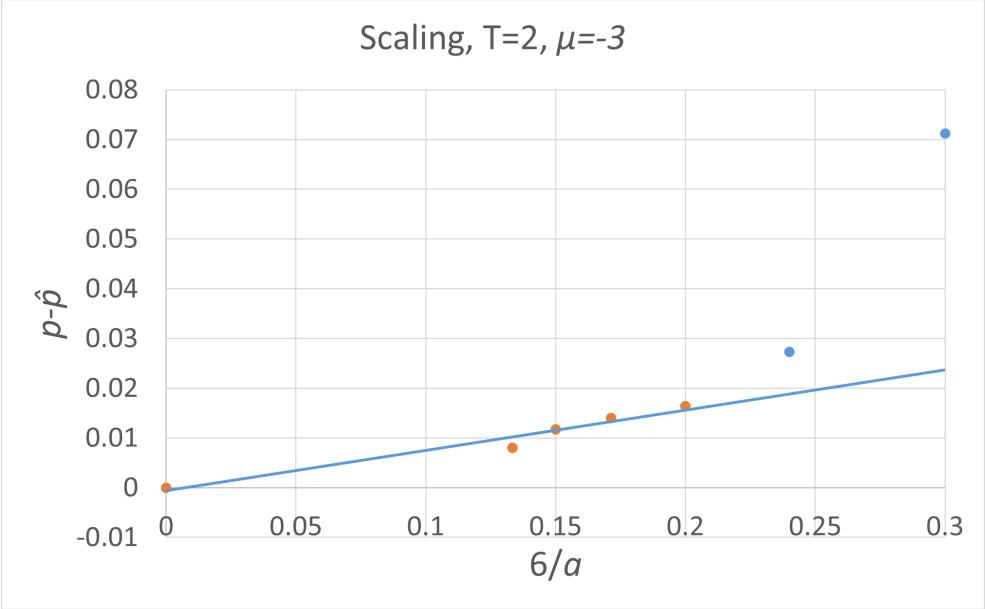

Figure 4.35: Using the scaling Law to compare the integral values

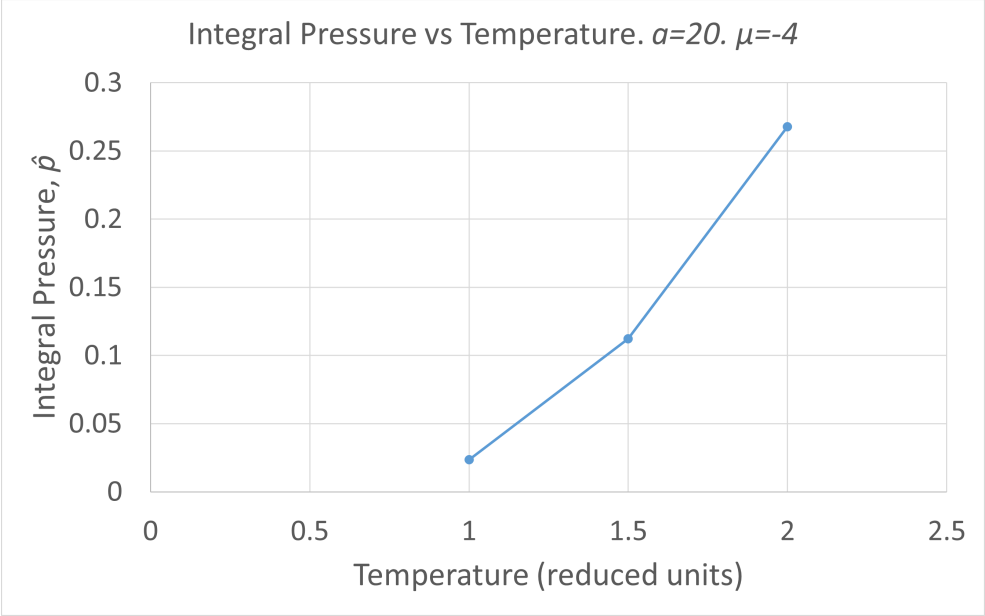

Figure 4.36: Graphing integral pressure $\widehat{p}$ against temperature T. For constant lattice constant $a = 20$ and constant chemical potential $\mu = -4$

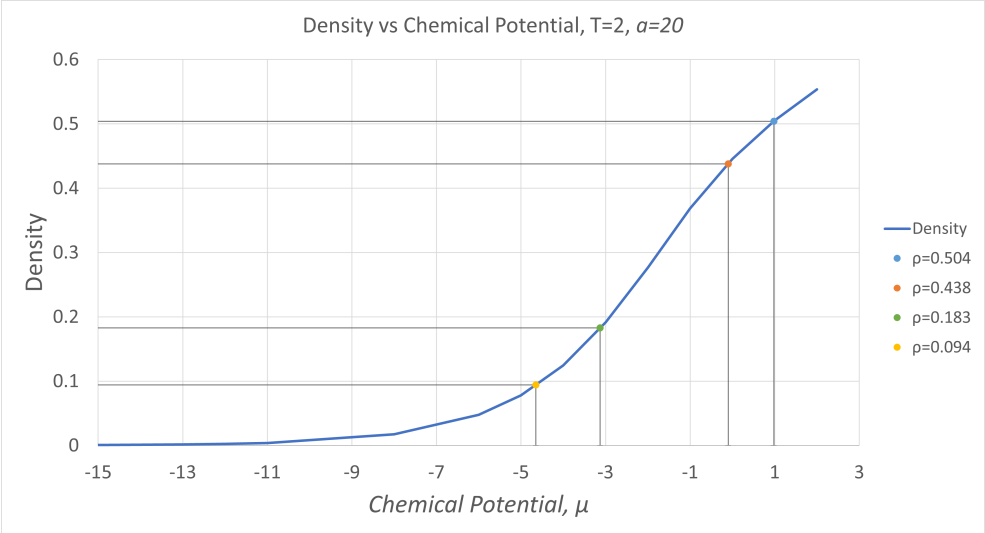

Figure 4.37: Getting the relevant μ values using the reference density values.

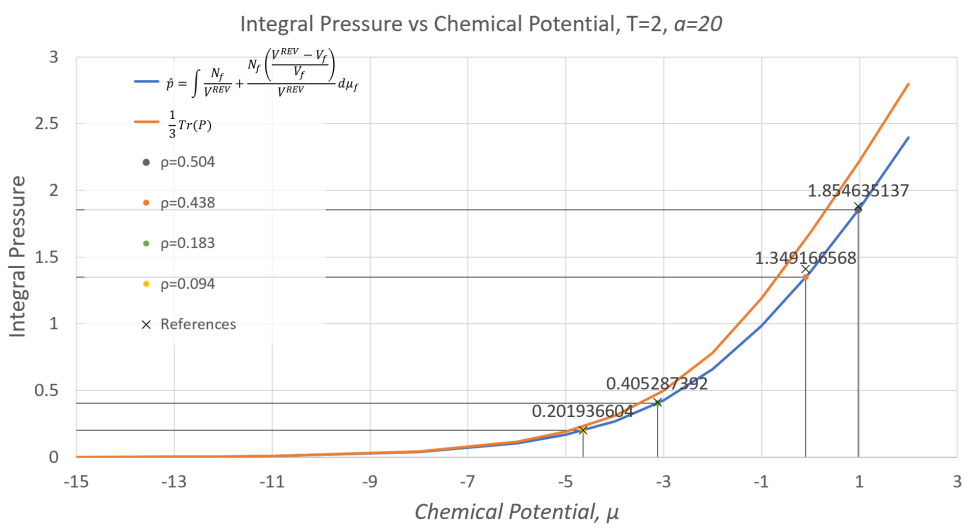

Figure 4.38: Checking the computed values against reference values. μ values of interest read from figure(4.37)

4.2.3 Discussion of Porous Medium Results

Lattice constant $a = 45$

Figure(4.14) shows us the density of the fluid particles in relation to its distance from a solid particle. This gives us a better understanding on how the Lennard-Jones potential is affecting the system. We see that there is lower density when the density is studied for a location closer to the solid particle, indicating that there is repelling force between the solid particles and the fluid particles. We also see that the density gets lower again when go far enough away from the solid particle. To understand this we can look at figures(4.12 and 4.13). The front-facing face-centered solid particle is the one we are measuring the density of the fluid particles around. By studying the density of the fluid particles in each shell with varying distance from the solid particle, we get the relative density of the fluid particles around the solid particle. Now to understand the dip in the density observed when moving away from the solid particle, as seen in figure(4.14), we notice that as the shells get further away from the solid particle we are studying, they are getting closer to other solid particles. The interaction between these solid and the fluid particles are going to be repelling as well, and thus we see the decline in the fluid density.

As observed previously, there is a repelling fore between the solid particles and fluid particles. Looking at figures(4.15 to 4.16) we see that the fluid density measured as a function of time, the density is consistently slightly lower for the FCC unit cell as compared to Bulk. Looking at figure(4.18) we see how the fluid density varies for the FCC unit cell for different temperatures. The units are all reduced units as described in table(3.1). Figures(4.20 to 4.21) illustrates the same, however as a function of chemical potential μ. The fluid density is consistently more for the Bulk compared the the FCC unit cell of same size, although the difference is less visible from the graphs. See figure(4.19) the difference more clearly. We see that the ratio between the Bulk and the FCC unit cell of the same size is mostly above 1, indicating that the fluid density in the Bulk system is slightly above that of the FCC unit cell. Figure(4.22) shows the difference in the fluid density different temperatures. We observe that the fluid density for the FCC unit cell increases with increasing temperature.

Our equation(2.46) gives the integral pressure as a function of chemical potential μ. We expanded upon the equation(2.37) to take into account the more

complex structure of the system. We did this by introducing V^{REV}. Further, we mentioned how the distance between the closest solid particles d were previously seen to affect the observed results. When $a = 45$ for the FCC unit cell, and the radius of the solid particles $r = 10\sigma$, d is greater than 11σ. Figures(4.23 to 4.24) shows the results from using the new method or equation(2.46) we formulated in the theory. Notice how in the case of the Bulk system, the equation()2.46 reduces back to equation(2.37) as $V_f = V^{REV}$. We see from the figures that the integral pressure $\widehat{p}$ nearly identical in both the Bulk and the FCC unit cell. The slight variation can be explained by the slight variation we observed in the density we discussed earlier. The result is as expected, given that d is greater than 11σ we were not expecting contributions from disjoining pressure. From figure(4.25) we observe that the integral pressure $\widehat{p}$ increases with temperature, this is consistent with the theory.

Lattice constant $a = 20, 25, 30$**.** $r = 5\sigma$

Figures(4.26 to 4.34) shows the results of integral pressure $\widehat{p}$ calculation of FCC unit cells with solid particle radius $r = 5\sigma$ for varying lattice constants and temperatures. The integral pressure was computed using both the new equation(2.46) and Trace of pressure tensor. We observe a trend where the the difference between the two increases with lower lattice constants, and higher temperatures. We use the scaling law discussed in the theory to look further into this. Figure(4.35) graphs the difference between the earlier mentioned pressure measurements against $6/a$. We see that for lattice constant above $a = 30$, i.e below 0.2 in $x-$direction. The values seem to scale linearly. But once a is below 30, it acts differently. This is likely due to contributions from disjoining pressure.

Figure(4.36) helps us consider the entropy density of confined fluid as discussed in theory. Looking at equation(2.51) we see that the slope of the graph gives us the entropy density. As one would expect from theory, the entropy density seems to increase with increasing temperature.

A fellow Master student provided with specific values from their system, where they were calculating the integral pressure in a different manner. These values can be seen in table(4.1). The values were for a porous medium system just like the one use in this paper, with FCC structure. The lattice constant $a = 20$, solid particle radius $r = 5\sigma$, temperature $T = 2.0$. In figure(4.37) we can read of the appropriate chemical potential values for the given densities in table(4.1). Then

in figure(4.38) we read of the integral pressure values for the chemical potential values we read off from figure(4.37). The values correspond with the reference values we were given with a percent error of 4.32% where the values deviates the most.

Table 4.1: Reference values for porous medium with FCC structure where lattice constant $a = 20$ and temperature $T = 2.0$ in reduced units. Values provided by Mina Sørensen Bratvold, and was collected from work done for her own Masters project.

Density	**Integral Pressure**
0.094	0.20
0.183	0.41
0.438	1.41
0.504	1.88

Chapter 5

Conclusion

The essential goal was to formulate a new method for describing the integral pressure of single-phase fluid in porous medium. We first applied the theory to slit pore and got satisfactory results. Then expanded upon it to formulate an equation for FCC unit cell.

From the work described in this paper, we have formulated a new way to compute the pressure in a nano-porous medium. We compute the integral pressure via chemical potential μ as formulated in equation(2.46). We have seen that this method works for slit pores as well. The results for the slit pores were calculated with a simpler equation(2.37). But the expanded version takes into account REV, thus facilitating for more complex structures such as the porous medium.

The work done here supports prior observations regarding the disjoining pressure being a factor for FCC lattices where the shortest distance between solid particles were shorter than $d = 11\sigma$, or rather that one could ignore it for d greater than 11σ.

We compared our results against reference values and saw that they corresponded well, within a percentage error of 4.3%.

The work was caried out by using molecular dynamics simulations of a single-phase fluid in a pore described as face-centered lattice of spherical grains in a pore. The tool was crucial for being able to test out the assumptions made in the theory.

Bibliography

[1] T. L. Hill, 'Thermodynamics of small systems,' *The Journal of Chemical Physics*, vol. 36, no. 12, pp. 3182–3197, 1962. DOI: 10.1063/1.1732447. eprint: https://doi.org/10.1063/1.1732447. [Online]. Available: https://doi.org/10.1063/1.1732447.

[2] D. Bedeaux, S. Kjelstrup and S. Schnell, *Nanothermodynamics: General Theory*. May 2020, ISBN: 978-82-691871-0-6.

[3] O. Galteland, D. Bedeaux, B. Hafskjold and S. Kjelstrup, 'Pressures inside a nano-porous medium. the case of a single phase fluid,' *Frontiers in Physics*, vol. 7, Apr. 2019. DOI: 10.3389/fphy.2019.00060. [Online]. Available: https://doi.org/10.3389/fphy.2019.00060.

[4] W. G. Gray and C. T. Miller, 'Thermodynamically constrained averaging theory approach for modeling flow and transport phenomena in porous medium systems: 8. interface and common curve dynamics,' *Advances in Water Resources*, vol. 33, no. 12, pp. 1427–1443, Dec. 2010. DOI: 10.1016/j.advwatres.2010.07.002. [Online]. Available: https://doi.org/10.1016/j.advwatres.2010.07.002.

[5] L. S. Bennethum and T. Weinstein, *Transport in Porous Media*, vol. 54, no. 1, pp. 1–34, 2004. DOI: 10.1023/a:1025701922798. [Online]. Available: https://doi.org/10.1023/a:1025701922798.

[6] J. J. Magda, M. Tirrell and H. T. Davis, 'Molecular dynamics of narrow, liquid-filled pores,' *The Journal of Chemical Physics*, vol. 83, no. 4, pp. 1888–

1901, Aug. 1985. DOI: 10.1063/1.449375. [Online]. Available: https://doi.org/10.1063/1.449375.

[7] B. D. Todd, D. J. Evans and P. J. Daivis, 'Pressure tensor for inhomogeneous fluids,' *Physical Review E*, vol. 52, no. 2, pp. 1627–1638, Aug. 1995. DOI: 10.1103/physreve.52.1627. [Online]. Available: https://doi.org/10.1103/physreve.52.1627.

[8] T. Ikeshoji, B. Hafskjold and H. Furuholt, 'Molecular-level calculation scheme for pressure in inhomogeneous systems of flat and spherical layers,' *Molecular Simulation*, vol. 29, no. 2, pp. 101–109, Jan. 2003. DOI: 10.1080/10286620210002518a. [Online]. Available: https://doi.org/10.1080/10286620210002518a.

[9] P. J. d. P. Atkins, *Atkins' Physical Chemistry [Paperback] [Mar 13, 2014] Atkins, Peter Julio de Paula.* English, Paperback. Oxford University Press, Jan. 2014, ISBN: 978-0199697403. [Online]. Available: https://lead.to/amazon/com/?op=bt&la=en&cu=usd&key=019969740X.

[10] O. Galteland, D. Bedeaux, B. Hafskjold and S. Kjelstrup, 'Pressures inside a nano-porous medium. the case of a single phase fluid,' *Frontiers in Physics*, vol. 7, p. 60, 2019, ISSN: 2296-424X. DOI: 10.3389/fphy.2019.00060. [Online]. Available: https://www.frontiersin.org/article/10.3389/fphy.2019.00060.

[11] O. Galteland, D. Bedeaux and S. Kjelstrup, *Nanothermodynamic description and molecular simulation of a single-phase fluid in a slit pore*, 2020. arXiv: 2012.00562 [physics.chem-ph].

[12] B. Hafskjold and T. Ikeshoji, 'Microscopic pressure tensor for hard-sphere fluids,' *Physical Review E*, vol. 66, no. 1, Jul. 2002. DOI: 10.1103/physreve.66.011203. [Online]. Available: https://doi.org/10.1103/physreve.66.011203.

[13] S. Plimpton, 'Fast parallel algorithms for short-range molecular dynamics,' *Journal of Computational Physics*, vol. 117, no. 1, pp. 1–19, 1995, ISSN: 0021-9991. DOI: https://doi.org/10.1006/jcph.1995.1039. [Online]. Available: http://www.sciencedirect.com/science/article/pii/S002199918571039X.

[14] B. Hafskjold, K. P. Travis, A. B. Hass, M. Hammer, A. Aasen and Ø. Wilhelmsen, 'Thermodynamic properties of the 3d lennard-jones/spline model,' *Molecular Physics*, vol. 117, no. 23-24, pp. 3754–3769, 2019. DOI: 10.1080/00268976.2019.1664780. eprint: https://doi.org/10.1080/00268976.2019.1664780. [Online]. Available: https://doi.org/10.1080/00268976.2019.1664780.

[15] D. Frenkel and B. Smit, *Understanding molecular simulation : from algorithms to applications. 2nd ed*. Jan. 1996, vol. 50. DOI: 10.1063/1.881812.

[16] A. Stukowski, 'Visualization and analysis of atomistic simulation data with OVITO–the open visualization tool,' *Modelling and Simulation in Materials Science and Engineering*, vol. 18, no. 1, p. 015 012, Dec. 2009. DOI: 10.1088/0965-0393/18/1/015012. [Online]. Available: https://doi.org/10.1088/0965-0393/18/1/015012.

Appendix A

Additional Material

A.1 Example LAMMPS input file

```
variable mu equal -3.000000
variable a equal 20.000000
variable          T equal 2.0
variable          d equal 4.0/$a^3.0
variable          L equal 1
variable          s22 equal 10.0
variable          R22 equal ${s22}-1.0
variable          s12 equal (1.0+${s22})/2.0
variable          R12 equal ${R22}/2.0

lattice           fcc $d
region            box block 0 $L 0 $L 0 $L

create_box        2 box
create_atoms      2 box

pair_style        lj/spline
pair_coeff        1 1 1.0 1.0 1.0 0.0
pair_coeff        1 2 1.0 ${s12} 1.0 ${R12}
pair_coeff        2 2 1.0 ${s22} 1.0 ${R22}

mass              * 1
```

```
variable          type atom type==1
dump              dump all custom 100 dump.out id type x y z
group             mdatoms dynamic all var type

compute           T mdatoms temp
compute           pe all pe
compute           ke mdatoms ke
compute_modify    T dynamic/dof yes
compute_modify    pe dynamic yes
compute_modify    ke dynamic/dof yes

variable          N equal count(mdatoms)

compute           peratom mdatoms stress/atom T

compute           p all reduce sum c_peratom[1] c_peratom[2] c_peratom[3]
variable          press equal -(c_p[1]+c_p[2]+c_p[3])/(3*vol)

variable          density equal count(mdatoms)/vol

variable          r equal 5.0
variable          vols equal (((4/3)*PI*(v_r*v_r*v_r)))
variable          volu equal vol-(v_vols*4)
variable          pressu equal -(c_p[1]+c_p[2]+c_p[3])/(3*v_volu)
variable          densityu equal count(mdatoms)/v_volu

fix               nvt mdatoms nvt temp $T $T 0.002
fix_modify        nvt temp T

fix               gcmc mdatoms gcmc 100 100 0 1 23624 $T ${mu} 0 full_energy

thermo_style      custom step c_T c_pe c_ke v_N pxx pyy pzz v_densityu v_pressu v_density v_press



thermo            100
timestep          0.002

run               600000
write_restart     cont.restart
```